INVESTIGATING THE IMPACTS OF PARTICLE SIZE AND WIND SPEED ON BROWNOUT

THESIS

Brandy A. Swanson, Captain, USAF

AFIT-ENP-MS-15-M-097

DEPARTMENT OF THE AIR FORCE
AIR UNIVERSITY

AIR FORCE INSTITUTE OF TECHNOLOGY

Wright-Patterson Air Force Base, Ohio

DISTRIBUTION STATEMENT A
APPROVED FOR PUBLIC RELEASE; DISTRIBUTION UNLIMITED.

The views expressed in this document are those of the author and do not reflect the official policy or position of the United States Air Force, the United States Department of Defense or the United States Government. This material is declared a work of the U.S. Government and is not subject to copyright protection in the United States.

AFIT-ENP-MS-15-M-097

INVESTIGATING THE IMPACTS OF PARTICLE SIZE AND WIND SPEED ON BROWNOUT

THESIS

Presented to the Faculty

Department of Engineering Physics

Graduate School of Engineering and Management

Air Force Institute of Technology

Air University

Air Education and Training Command

in Partial Fulfillment of the Requirements for the

Degree of Master of Science in Applied Physics

Brandy A. Swanson, B.S., M.A.

Captain, USAF

March 16, 2015

DISTRIBUTION STATEMENT A
APPROVED FOR PUBLIC RELEASE; DISTRIBUTION UNLIMITED.

AFIT-ENP-MS-15-M-097

INVESTIGATING THE IMPACTS OF PARTICLE SIZE AND WIND SPEED ON BROWNOUT

THESIS

Brandy A. Swanson, B.S., M.A.
Captain, USAF

Committee Membership:

Lt Col Robert S. Wacker, PhD
Chair

Lt Col Kevin S. Bartlett, PhD
Member

Steven T. Fiorino, PhD
Member

Abstract

The impact of particle size and wind speed on brownout cloud development was investigated for various rotary wing aircraft using Continuum Dynamics, Inc. (CDI) Brownout Analysis Tool, a high physical fidelity brownout model used by both U.S. Army Aviation and National Aeronautics and Space Administration (NASA) for rotorwash analysis. Simulations were run for over 125 different combinations of particle size, wind speed, and aircraft type, then output data was post-processed to determine a transmissivity, and ultimately a visibility value, that could be used in developing a severity metric for the brownout clouds generated. For most aircraft types evaluated, stronger wind speeds and smaller particle diameters resulted in denser clouds. Wind speeds greater than 6 m s^{-1} were required to lift very coarse sand.

Table of Contents

Page

List of Figures

List of Tables

INVESTIGATING THE IMPACTS OF PARTICLE SIZE AND WIND SPEED ON BROWNOUT

I. Introduction

1.1 Rotary Wing Brownout Definition

Helicopter brownout is a phenomenon that occurs during takeoff, landing, and near-ground hover when spinning rotor blades create a cloud of dust that is thick enough to inhibit visibility and cause spatial disorientation. Essentially aircraft-induced dust storms, brownout results from strong rotor downwash velocities dislodging loose dust or sand in the wake of the aircraft. These aircraft-induced dust clouds not only have potential to cause significant and costly damage to helicopter engines and rotor systems, but are extremely dangerous for aircrews. Brownout occurs on short time and spatial scales when atmospheric and surface conditions are favorable.

The potential for rotor downwash exists in arid regions with a sufficient supply of dry, loose, fine dust or sand. Depending on the aircraft's ability to elevate the particles initially and re-circulate them once aloft, a sizeable and optically thick cloud of dust can be generated near the ground. Many factors go into determining ideal surface conditions for brownout potential, including soil type and moisture, surface roughness, and particle size. The size and weight of the rotary wing aircraft, its speed and its trajectory at low-altitudes also play a large role on the aircraft's susceptibility to brownout. Modeling the interaction between different airframes and land surface types while determining ideal conditions for particle entrainment, transport, and

saltation requires a significant level of knowledge of dust particle physics, radiative transfer, and aerodynamics.

1.2 Objectives

Currently, operational Air Force weather forecasting does not include an analysis of brownout potential for rotary wing operations. The Air Force Weather Agency (AFWA) produces forecast tools for predicting dust storms and dust emission, and has been working toward developing an algorithm for a brownout potential forecast product. The product needs to model dust entrainment and transport processes, and also account for particle radiative characteristics and aerodynamic influences. While dust emission and entrainment processes are similar for both wind-induced dust storms and aircraft-induced brownout clouds, the aircraft impact on the force balance in the vertical direction needs to be factored into the equations for brownout, which proves to be challenging. Numerical weather prediction models are typically run on a large scale to enable global coverage, but brownout occurs on a very small spatial scale and is airframe and land surface dependent.

Knowing how and why brownout occurs is critical to detecting susceptible regions, applying that knowledge at the mission/tactical level, and improving weather support to rotary wing operations. The objective of this study is to investigate the effect of particle size and wind speed on brownout cloud generation and evolution for a variety of different rotary wing aircraft types using a brownout simulation and analysis tool developed by Continuum Dynamics, Inc. (CDI). One goal is to produce a detailed brownout risk assessment matrix that can be used in the creation of an NWP-based brownout potential algorithm, and eventually a brownout prediction tool. Successful development of this matrix has the potential to provide updated guidance to AF weather personnel and the insight gained may improve local weather prediction in

the future by including an analysis of brownout potential where applicable. The ultimate goal of this research is to provide a usable product for forecasting rotory wing brownout potential that can be useful for AF implementation into operational weather forecasting for both AF and Army rotary wing operations.

1.3 Document Outline

The following chapters of this thesis contain background information, research methodology, results, analysis, and conclusion. Background information presented in Chapter II includes a discussion of dust source regions, particle entrainment and transport, physics of rotorcraft brownout, an overview of the CDI Brownout Analysis Model, an overview of numerical weather prediction (NWP) dust modeling. Chapter III outlines the method for post-processing the brownout cloud characteristics and the development of a brownout cloud severity metric. An analysis of the output produced from the model and its post-processing is detailed in Chapter IV. Lastly, Chapter V summarizes the results of this research and suggests additional topics for future work. Each of these sections incorporates information identified in previous chapters and assumes a small working knowledge of dust particle physics.

II. Background

Quantitative estimates of dust emission rate are rather difficult due to the complexity of modeling dust emission and dust transport. Emission is determined by an interacting set of processes including weather (high wind and minimal rainfall), soil state (age and moisture), and surface roughness (vegetation and larger grains impeding wind erosion), while transport depends upon the interactions between particles and on turbulence in the atmospheric boundary layer (Lu and Shau 2001). The intricacies of all of the dynamic processes at play during a brownout event or dust cloud generation, coupled with the small spatial scale upon which these events occur, make characterizing and modeling such events challenging. While differences in each variable at play are acknowledged, it is often necessary to parameterize when possible to arrive at a solution in a timely manner. Preserving the integrity of the physical and dynamic processes and variables is important in modeling and forecasting brownout, and dust storms, but it must also be noted that certain assumptions must be made when solving the equations of motion for a given brownout scenario. The next section details the variables, key factors, and concepts of dust emission and transport and gives the reader a general idea of how rotary aircraft brownout can be modeled.

2.1 Dust Sources or Source Regions

Perhaps one of the most important elements in determining brownout potential is the dust source region itself. Obviously dust storms and brownout aren't possible without a significant amount of dust available. Determining the types and locations of the more fertile source regions around the world has been an area of major study for several years. From taking soil samples on the ground at numerous grid points (a very time-consuming process) to using remote sensing tools to characterize the

different properties of soils that are known to have a high lofting potential, considerable resources have been devoted to capturing the soil state of regions of interest around the world. Finding these highly productive dust hot spots, whether in situ or by remote sensing, has been pivotal in the advancement of dust modeling. The following sections explain soil characteristics and elucidate why certain landform and soil types are more susceptible than others.

2.1.1 Soil Types.

The United States Department of Agriculture (USDA) Natural Resources Conservation Service (NRCS) recognizes and distinguishes between over 20,000 different types of soils in the U.S. alone in its Soil Taxonomy (USDA/NRCS 2014). While a basic understanding of soil types is needed to fully appreciate the various impacts on dust lofting and circulation, an exhaustive review of each soil series and group is impractical. A simple overview of soils will suffice for the purposes of this study. Every soil type is a mixture of sand, silt, clay, and organic material, classified based on its size and texture. Sand is the largest of the particle materials, with radii up to 2 mm; it feels gritty and doesn't retain water easily. The large spacing between grains allows for drainage and drying and causes the particles to be less cohesive. Silt is the next largest material, ranging between 0.05-0.002 mm. It has the general consistency of flour, finer than sand but still gritty. Found commonly in dry riverbeds or floodplains, this material is easily erodible and is often blown downstream by dust storms. The smallest soil component is clay, with particle sizes less than 0.002 mm. Ultra-fine in texture, clay feels sticky when wet, is extremely cohesive, and does not allow air to move through it easily. Clay makes a soil dense and is hard as concrete when dry. Loam is a nearly even mixture of sand and silt with a smaller amount of clay. Spaces between particles are large enough to allow water to flow in and the

small amount of clay helps the particles stick together (USDA/NRCS 2014).

2.1.2 Particle Size.

The USDA distinguishes between rock fragments, like gravel and pebbles, and fine earth (sand, silt, or clay) based on the size of the particle. Table 1 outlines the size categories the USDA uses as a basis for distinguishing types of sand and dust.

Table 1. Soil categories by particle size from USDA Soil Survey Manual (2014)

Type	***Size***
Very coarse sand	2.0-1.0 mm
Coarse sand	1.0-0.5 mm
Medium sand	0.5-0.25 mm
Fine sand	0.25-0.10 mm
Very fine sand	0.10-0.05 mm
Silt	0.05-0.002 mm
Clay	<0.002 mm

It is also important to note that while sand and dust are used somewhat interchangeably when it comes to describing and defining soils and brownout, there exists an important distinction between the two. In geological sciences, both sand and dust are solid particles that were created from the weathering of rocks. In atmospheric sciences, however, dust is material that can be lofted and suspended by the wind whereas sand remains on the ground.

2.1.3 Soil Moisture.

Water binds soil particles together by filling in the gaps between the grains (Hillel 2004). A soil's moisture content depends on its capacity to hold water. Sand, for instance, can hold less than silt or clay because of the larger gaps between particles, which allows free drainage of water (Fecan et al. 1999). Increased moisture equates to increased cohesion of the material, which leads to delayed release of solitary particles

and also increases the threshold friction velocity, or speed necessary to pull a grain from the surface (Haehnel et al. 2013). Increased soil moisture creates tighter bonds between particles and adds weight to the material, requiring higher wind speeds in order to overcome cohesive and gravitational forces.

2.1.4 Surface Roughness.

A surface can contain elements that make it more resistant to particle entrainment such as vegetation or heavier stones and gravel. Such features, often referred to as roughness elements, provide a protective cover to the soil below by absorbing momentum from the wind that would have caused the smaller, lighter particles to loft and be entrained (Bacon et al 2011). The concentration of roughness elements has a considerable impact on the lofting potential of particles of a given surface type (Wolfe and Nickling 1993).

2.2 Particle Entrainment and Transport

Atmospheric conditions are almost as important as land surface conditions in determining the propensity of different landscapes to produce dust. In the absence of strong winds, or in the aftermath of a substantial amount of precipitation, the ideal landform for dust lofting may be unable to release any particles from the surface for entrainment.

Aeolian processes refer to wind-driven emission, transport, and deposition of sand and dust. In order for aeolian processes to take place, there must be a dust source region with a sufficient supply of fine earth material and a strong enough wind to be able to break those particles from the surface (Nickling 1994; Zender et al. 2003). The next few sections explain lifting mechanisms and wind speeds required to lift particles of different masses, saltation (or bouncing) of particles against one another

after being lifted from the surface, transport mechanisms, and deposition of different particles and their effect on the atmosphere.

2.2.1 Lifting.

In order for particles to be lifted initially, the wind needs to be strong enough to pull loose fine earth material from the surface. How strong that wind needs to be is a function of gravitational force and the cohesive forces between particles. Threshold friction velocity is the point at which aerodynamic forces overcome gravity and cohesive forces between particles, allowing entrainment of loose material.

Figure 1 depicts the forces acting on a stationary dust particle resting on a bed of other particles (Kok et al 2012; Shao and Lu 2000). P denotes the pivot point or point of contact with the particle's supporting neighbor, F_L is the lifting force, F_g is the gravitational force, F_{ip} is the inter-particle cohesive force, F_d is the aerodynamic drag force, and r_d, r_g, and r_{ip} are the moment arms associated with each force. When all forces acting on the particle sum to zero, it is then able to be carried along by the wind. Entrainment occurs when the drag and lifting forces just barely exceed the gravitational and inter-particle cohesive forces (Iversen et al. 1976; Shao and Lu 2000; Kok et al 2012). An expression can be derived for the force balance at the moment of lifting:

$$r_d F_d \approx r_g(F_g - F_L) + r_{ip}F_{ip} \tag{1}$$

where

$$F_d = K_d \rho_a D_p^2 u_*^2 \tag{2}$$

$$F_g = mg = \pi/6(\rho_p - \rho_a)gD_p^3 \tag{3}$$

$$\tau = \rho_a u_*^2 \tag{4}$$

The air density is denoted by ρ_a and particle density by ρ_p, g is the acceleration

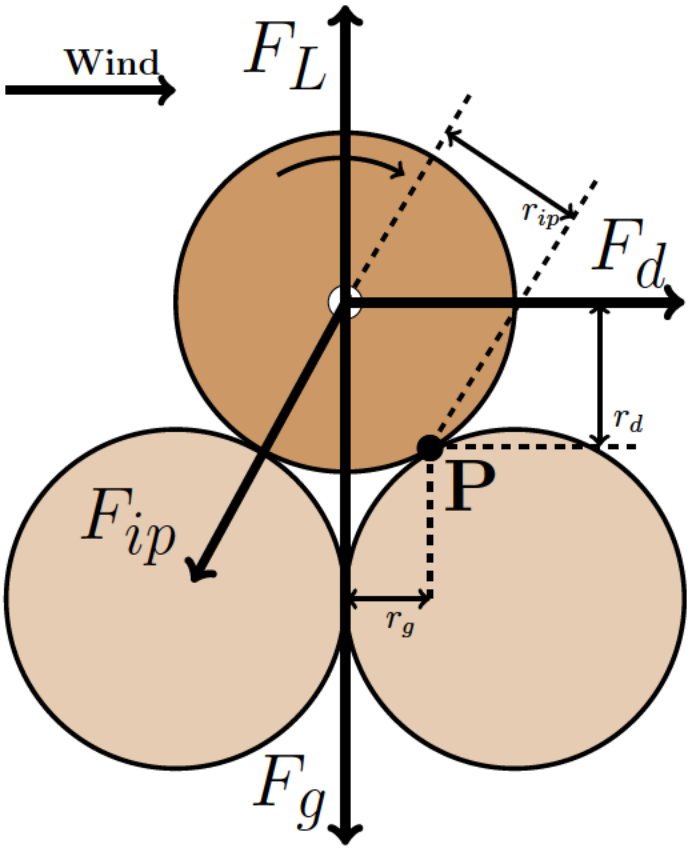

Figure 1. Diagram of forces acting on a particle sitting at rest in a particle bed. Forces are denoted by thick arrows, and their moment arms relative to the pivoting point P are indicated by thin arrows. When the moment of the aerodynamic lift and drag forces exceeds that of the gravitational and inter-particle forces, the particle will be entrained into the flow by pivoting around P in the indicated direction (adapted from Kok et al, 2012).

due to gravity, K_d is a dimensionless drag coefficient of the order of approximately 10 (Iversen et al. 1976), u_* is the shear velocity, D_p is the diameter of the particle, and τ is the fluid shear stress. Solving for the threshold friction velocity, u_{*t}, yields (Bagnold 1954):

$$u_{*t} = A_{fl}\sqrt{(\rho_p - \rho_a)/(\rho_a g D_p)} \tag{5}$$

where A_{fl} is a proportionality constant that is a function of the lift force, the inter-particle cohesive force, and the Reynolds number of the flow (Iversen et al. 1976).

2.2.2 Saltation.

After lifting, particles bounce along the surface and collide with each other, kicking up or freeing more particles (Kok et al. 2012). Saltation is the bouncing motion of windblown grains across an underlying granular surface, and is also the principle mechanism for sand and soil transport (Shao and Raupach 1992). Once a particle is lifted, saltation can have an impact on the dust lofting and amount and types of dust and sand being entrained. Saltators have the ability to mobilize larger grains that may have otherwise been stationary by colliding with them and transferring momentum. Often, the cohesive forces between particles are strong enough to prevent lifting by just the wind alone. It is here that saltation plays a critical role by breaking the cohesive bonds between particles, allowing them to be lifted and entrained. It is necessary to have more than just ultra-fine particles for entrainment; saltation requires slightly larger grains for effective transfer of momentum (Sweeney et al. 2011).

Saltation not only aids the lifting process by mobilizing particles of various sizes, it also helps keep airborne grains aloft with inter-particle interactions. Dust emission can happen through three distinct processes (Shao 2000): (a) direct aerodynamic entrainment, (b) expulsion of dust particles from soil aggregates by impact of saltating particles, or (c) ejection of dust particles by soil aggregates engaged in saltation (Kok et al. 2012). The last two processes are a result of saltation bombardment, which leads to sandblasting, the freeing of dust particles from aggregates that are either saltating or impacted by saltators (Gillette 1974; Shao 2004).

2.2.3 Transport and Circulation.

Once particles are ejected from the surface, either by direct aerodynamic lifting or by saltation bombardment, they can be transported by advection, convection, or turbulent mixing (Ginoux et al. 2001; Chin et al. 2000; Allen et al. 1996).

Advection is the movement of dust particles by the wind itself. Convection is a slightly more complex process that involves thermals, rising towers of buoyant air. These ascending towers entrain dust particles, mixing them into the environmental flow to be carried downstream. Turbulent mixing happens due to shear-induced eddies in the atmospheric boundary layer. Viscosity causes wind velocity to go to zero at the surface so even weak winds will tend to drive some amount of mechanical shear just above the surface, creating small-scale turbulent eddies. As with convective eddies, these shear-induced eddies entrain dust particles into the environmental wind (Holton 2004; Chin et al. 2000; Allen et al. 1996).

2.2.4 Deposition.

Dust particles are removed from the atmosphere after entrainment by either dry deposition or wet deposition. Dry deposition is due to the combination of gravitational settling and eddy diffusion. Wet deposition includes both precipitation collecting dust particles as it falls and dust particles serving as condensation nuclei in the formation of clouds (Kok et al. 2012; Zender et al. 2003; Ginoux et al. 2001). Larger particles tend to leave the atmosphere through gravitational settling, with heavier grains requiring higher winds to keep them aloft. Wet deposition usually dominates for particles smaller than 5 μm (Miller et al. 2009; Zender et al. 2003). Only very small particles (≤ 0.2 μm) are able to be suspended in the air for substantial periods of time (Miller et al. 2009; Zender et al. 2003; Kok et al. 2012). The arrival of foreign dust aerosols in a region has a significant impact on the environment in that area. Mineral dust aerosols can contain chemicals that have the potential to affect weather and climate, ecosystems, public health, the hydrologic cycle, and agriculture.

2.3 Physics of Brownout and Aerodynamics

The discussion to this point has been applicable to both dust storms and rotor wash, but now a distinction will be made in how an aircraft-induced dust cloud is specifically impacted by the characteristics of the helicopter. Different rotor speeds and configurations, airframes, and flight paths can all vary the severity of a brownout event. This section discusses those factors and the radiative properties of the brownout cloud itself.

2.3.1 Helicopter Downwash Velocities.

Helicopter rotor systems create lift by displacing air downward. Rotor blades have a flat bottom edge and a curved top edge. When rotor blades spin, a low pressure area forms above the blade and high pressure below, supplying lift to the vehicle. The amount of lift is controlled by the speed of the blades and the angle at which they meet the incoming air flow. Pitch is increased during takeoff to produce enough lift to overcome the weight of the aircraft and pitch is decreased during landing so that the weight of the aircraft exceeds the amount of lift produced. In order for a helicopter to hover, lift must equal the weight of the airframe (Tanabe and Saito 2009). In all cases, the upward momentum imparted to the helicopter is opposed by an equal amount of downward momentum imparted to the air beneath it. The induced downwash velocity can be estimated using simple momentum theory and equation (6):

$$v = \sqrt{mg/(2\rho\pi R^2)} \tag{6}$$

where m is the mass of the aircraft, is the air density, and R is the rotor radius (Tanabe and Saito 2009). A UH-60 Blackhawk with a mass of 11,300 kg would then have an induced downwash velocity of about 27.5 m s^{-1} and a CH-47 Chinook with

24,500 kg would have an induced downwash velocity of about 28 m s^{-1}.

U.S. Army Aviation researchers found that the distribution of dust around a helicopter in a brownout cloud is a function of the number of rotors, disc loading (i.e. the weight of the aircraft), hover height, and the physical characteristics of the soil (Rodgers 1968). They found that the highest dust concentrations were in the vicinity of rotor blade overlap and that takeoff and landing maneuvers increased dust cloud concentration threefold (Rodgers 1968).

2.3.2 Scattering due to Brownout Clouds.

Atmospheric aerosols and dust particles within a brownout cloud absorb and scatter incident light, impairing visibility. The severity of the brownout event itself is directly proportional to the amount of light extinction by the cloud particles. Essentially, we want to find out how efficient the lofted dust particles are at absorbing and scattering light. The degree of extinction by scattering and absorption of light propagating through a small particle cloud is a function of particle size, number density, and optical properties (van de Hulst 1981). If a brownout cloud is viewed as a semi-infinite cloud, meaning it is so thick that a photon of light has a greater chance of being absorbed or scattered by the dust particles than it does of making it all the way through the cloud (Petty 2004), then we can use equation (7) to characterize the attenuated light intensity, or radiance:

$$I = I_0 e^{-\gamma\tau} \tag{7}$$

where I_0 is the incident light intensity, τ is the distance along the light's path, and γ is the extinction coefficient (Wachspress et al. 2008). The extinction coefficient γ

can be calculated using equation (8):

$$\gamma = \pi r^2 \rho Q \tag{8}$$

where r is the particle radius, ρ is the particle (number) density, and Q is the particle extinction efficiency factor, which takes into account the scattering direction, optical properties of the particles, and spectral characteristics of the incident light (Wachspress et al. 2008). It is important to note that these expressions take a very simplistic view of the interaction between photons and dust particles. Rigorously modeling a brownout cloud involves a far more complex approach that factors in multiple scattering, reflection, and radiance effects (Petty 2004). The Air Force Institute of Technology Center for Directed Energy (AFIT/CDE) Laser Environmental Effects Definition and Reference (LEEDR) model uses brownout optical properties to make these calculations without oversimplifying the physics of scattering, reflection, and absorption. Marek (2009) developed a technique to measure optical properties of brownout clouds for modeling terahertz propagation using the LEEDR model.

2.3.3 Computational Fluid Dynamics.

Computational fluid dynamics (CFD) uses numerical methods to analyze problems involving fluid flow. The Navier-Stokes equations and Euler equations (when not considering viscous force or interactions) are the fundamental equations used in CFD applications related to brownout due to their ability to resolve turbulent flow. In modeling the entrainment of dust particles, the two most important factors to consider are fluid threshold velocity (the velocity that is required to lift particles from the surface) and the flux rate of those particles into the flow field.

Eulerian transport models track particles through space and time from a fixed reference frame. Models of this type use the Euler equations or conservation of mass,

momentum, and energy to arrive at a solution. While use of conserved variables is computationally efficient, it fails to take into consideration changes following each particle. In a Lagrangian transport model, trajectories of individual particles are followed as they move through space and time. This can be computationally expensive, as the dynamics of each particle in the dust cloud must be modeled. It is possible, though, to obtain a fairly accurate solution by tracking a smaller group of representative dust particle clusters if a relatively homogeneous ground layer is assumed. This significantly reduces the computation time and allows for timely results, but restricts the solution to a single particle size.

2.4 Brownout Model Overview

Modeling the generation of a dust cloud in the wake of helicopters during take-off and landing has been an area of research interest for several years in both the civilian and military meteorological communities. A considerable number of aircraft accidents due to brownout have been reported in Iraq and Afghanistan since 2000, an issue that the military is working diligently to combat. Involvement in conflicts in desert regions has driven a need for better training tools and simulation software to prepare aviators for dangerous brownout situations before facing them firsthand in the deployed environment. Training aircrews on safely navigating through significant amounts of dust as well as safely landing while engulfed in a brownout cloud is one approach the aviation community is taking in lessening the number of brownout incidents.

While several brownout simulation tools exist, few lack the sophistication to accurately model the complexities of dust cloud generation and lifecycle. Using rudimentary software not only does little in preparing pilots and aircrew for real-time scenarios, it paints an unrealistic picture of the particulars of the brownout cloud,

which could potentially lead to counterproductive training. Continuum Dynamics, Inc. (CDI) has worked with the U.S. Army and NASA to develop a physics-based model that simulates dust cloud generation and evolution in the wake of rotary-wing aircraft. This section discusses the particulars of this model, its use in the field, the inputs it requires, and the output it produces.

2.4.1 The Continuum Dynamics, Inc. (CDI) Model.

As the name implies, CDI's Rotorcraft Brownout Analysis and Flight Simulation tool is both a high physical fidelity brownout analysis tool for research in aerodynamics and brownout mitigation and a brownout model that can be used in real-time flight simulations for pilot training. This specific software is a conglomeration of several applications previously developed by CDI including its Comprehensive Hierarchical Aeromechanics Rotorcraft Model (CHARM) coupled rotary-wing free wake, fast panel fuselage, ground surface model; its Multiple Aircraft Simulation Tool (MAST) flight simulation that models rotorcraft transient maneuvering flight near the ground for general wind conditions; its Lagrangian Deposition and Trajectory Analysis (LDTRAN) particle entrainment and transport model; its Visual Scattering and Obscuration (VISOR) model; and its OpenSceneGraph Brownout (OSGB) 3D multi-viewpoint brownout cloud rendering model (Wachspress et al. 2008). Figure 2 shows an OpenSceneGraph animation for a UH-60 simulation run with a 30 μm particle size in windless conditions.

2.4.2 CDI Model Applications.

Both NASA/Ames Research Center and the U.S. Army have implemented CDI's model for use in research and training (Wachspress et al. 2008). NASA/Ames uses the analysis module to study aerodynamic factors affecting brownout cloud generation

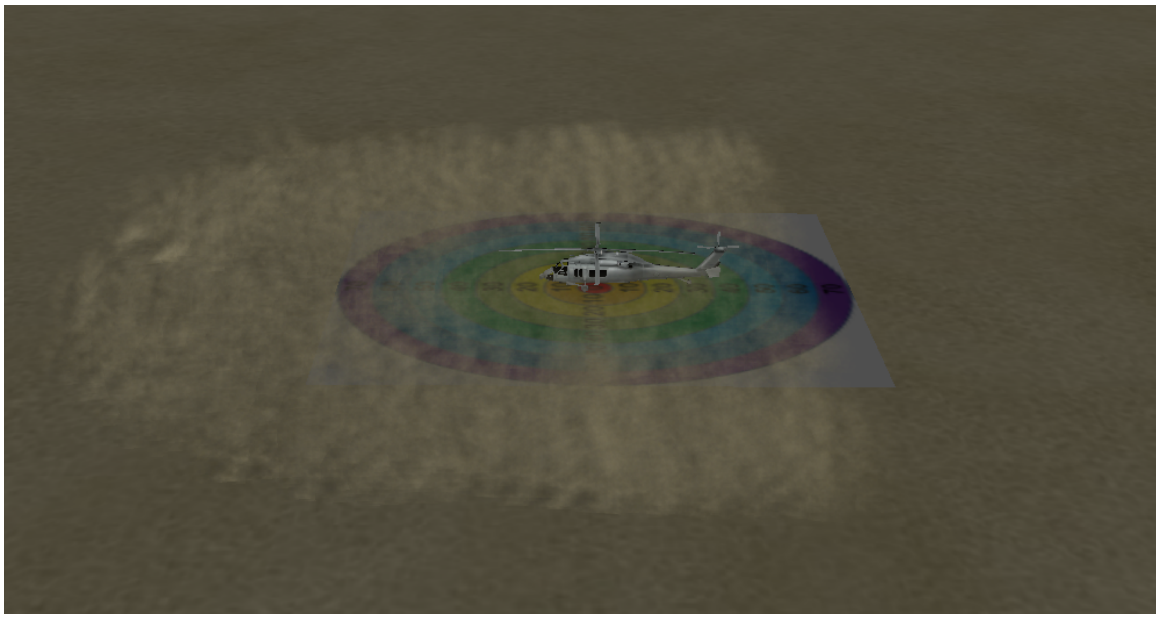

Figure 2. OpenSceneGraph rendering of a dust cloud simulation of a UH-60 helo landing to the west and the apparent dust cloud created.

and evolution. CDI's real-time brownout simulation tool has also been incorporated into rotorcraft flight simulation at the U.S. Army Advanced Prototyping Engineering and Experimentation (APEX) lab in Hunstville, AL. The brownout module was successfully integrated and demonstrated within the APEX laboratory Battlefield Highly Immersive Virtual Environment (BHIVE) simulation for use in U.S. Army piloted rotorcraft flight simulation (Wachspress et al. 2008).

2.4.3 CDI Model Inputs and Outputs.

The CDI brownout module receives input, through MATLAB subroutine calls during simulation runtime and from user-specified settings entered in the prompt window during execution. The subroutines contain data and variables necessary for most calculations but the user has the option to make modifications during each run before completing the simulation. The user is able to vary the aircraft type, wind magnitude and direction, the rotor positions and orientations, and the types of particles on the ground. The host can modify the subroutines or input files provided

during installation and can also change the resolution of the output if desired.

After running the brownout module, the user is presented with an animated solution of a brownout cloud rendered in the flight simulation. Two specific output files are generated by the module the Brownout Cloud Output File (brownout.out) describes the brownout cloud and the Aircraft Trajectory Output File (traj2.out) describes the aircraft trajectory. A sample of the brownout.out output file for a CH-47 simulation run with a $10\mu m$ particle size and no wind is shown in Table 2. CDI uses OpenSceneGraph to display an animation of the solution but quantitative values for particle cluster information can also be found in the Brownout Cloud Output File for use in post-processing.

Table 2. Sample brownout.out output file from a CH-47 simulation run using 10 μm particle size and no wind

Cluster	*Time*	*X Pos*	*Y Pos*	*Z Pos*	*Std Dev*	*Trans*
1588	18.500	14.100	-7.747	1.969	1.181	0.071
1589	18.500	12.148	-10.035	0.700	1.331	0.073
1590	18.500	9.669	-12.241	2.954	1.262	0.065
1591	18.500	6.123	-11.542	0.378	1.060	0.051
1592	18.500	3.490	-11.148	1.453	1.265	0.104
1593	18.500	0.891	-10.982	2.368	1.177	0.234
1596	18.500	-4.310	-0.765	0.976	1.154	0.652
1599	18.500	0.749	10.866	1.543	1.123	0.088
1600	18.500	3.007	10.599	1.872	1.189	0.091
1601	18.500	5.918	10.070	1.478	1.197	0.103
1602	18.500	8.197	9.660	2.401	1.111	0.156
1603	18.500	11.539	7.606	1.899	1.102	0.137
1604	18.500	12.441	4.872	1.969	1.181	0.222
1605	18.500	13.487	0.320	1.937	1.190	0.071
1606	18.500	-1.593	7.296	1.969	1.181	0.071

The first column of the following table lists the particle cluster by number, which is tracked throughout the simulation. The second column is the time step in seconds. The third through fifth columns represent the x, y, and z positions of the particle cluster in meters from the landing point. The second column from the right shows

the standard deviation of the particle distances from the center of the cluster and the rightmost column contains the particle cluster's transparency from 0 to 1, with 0 being opaque and 1 being transparent.

2.5 Numerical Weather Prediction Dust Modeling

Dust production by means of atmospheric forcing can be modeled but requires parameterization of dust source regions since a detailed and accurate mapping of the soil types and abundance does not exist. Utilizing dust source region (DSR) parameterization schemes allows numerical weather prediction models to account for variability in land surface characteristics, improving forecast accuracy. DSR schemes parameterize the physical processes related to soil binding that are too complex and computationally expensive to explicitly model. Several parameterization schemes have been developed to characterize the erodibility of soils, including land use-based, topography-based, hydrology-based, empirically-based, and surface reflectance-based methods. Currently, all operational Air Force Weather Agency (AFWA) dust transport models use either 1 degree or 1/4 degree resolution topography-based DSR maps. This method, while efficient and generally representative, neglects the contributions of small scale dust source regions like dry river beds or alluvial plains which can often be excellent dust producers. In an effort to move toward higher resolution modeling, AFWA has worked to dynamically tune its topography-based erodibility field by using dust enhanced satellite imagery and surface observations to locate plume head locations, then incorporating those fertile regions in the DSR mapping scheme (Jones 2012).

III. Methodology

This chapter outlines the methods used to obtain and analyze the data used in this study. In this chapter, the procedure used for generating the brownout cloud/particle clusters using CDI's Brownout Simulation and Analysis Model and the plan for post-processing the brownout cloud characteristics and output data are discussed. Also, the development of a metric used to assess the severity of the brownout cloud is detailed.

3.1 Generating Brownout Cloud Particle Clusters

Simulations were run for a total of 125 different combinations of aircraft, wind speed, and particle size. The five aircraft types used include the UH-1H, UH-60, CH-47, CH-53, and AH-64. The reason for choosing a variety of aircraft types was to investigate the varying aerodynamic influences of different sizes of helicopters and different rotor configurations. The UH-1H is the lightest aircraft at just under 4,500 kg and has a two-bladed main and tail rotor system. The UH-60 features a four-bladed main and tail rotor system and has a mass of about 10,000 kg. The AH-64 also has a four-bladed main and tail rotor system but less mass than the UH-60 at 8,000 kg. The heaviest aircraft type chosen is the CH-53, with a mass of about 15,000 kg. It has a six-bladed main rotor and a four-bladed tail rotor. The CH-47 was chosen for its unique three-bladed twin rotor system; it has an average mass of approximately 12,000 kg (Ghosh et al. 2010). The choice of aircraft also represents a cross-section of rotary-wing missions. Utility, or UH-type, helicopters have many uses including force movement and medical transport. Cargo, or CH-type, helicopters are used to ferry troops and supplies. Attack, or AH-type, helicopters are used for air assualt missions.

The wind speeds tested varied from 0 m s^{-1} to 12 m s^{-1} at 3 m s^{-1} intervals. Although there is rarely an instance with absolutely no atmospheric wind, the zero value was chosen to evaluate the aerodynamic influences on the brownout cloud in the absence of any wind and was used as a baseline for comparison. The cap of 12 m s^{-1} (approximately 24 knots) was chosen because that is on the higher end of safe wind speeds for most rotary-wing operations. Wind direction was fixed to a head wind (from 0 degrees) for all simulation runs. The range of particle sizes tested ranged from 10 μm to 90 μm, at 20 μm intervals. Fine desert sand is typically on the order of 10 μm, but since ground cover is not homogeneous, larger particle sizes were examined in this study to evaluate their impact on brownout clouds. Each particle size had to be evaluated individually as the model assumed a homogenous layer of particles at simulation start. Initial ground conditions included a 1-cm thick particle bed with 41 particle clusters in the X direction and 41 particle clusters in the Y direction. The particle bed was 60 m by 60 m with the aircraft centered over the landing point.

The user has the option to specify the trajectory of the helicopter during simulation. In order to remain consistent and to simplify geometry, a vertical descent trajectory was chosen. During this approach, the aircraft descends vertically at a constant rate from 15 m above the ground at simulation start to 1.5 m above the ground at 20 s.

3.2 Post-processing of Brownout Cloud Characteristics

After running each simulation, an output file was generated containing the data on particle clusters within the brownout cloud. Each particle cluster is numbered and tracked throughout the 20 second simulation at an interval of 0.01 s. The x, y, and z position in the inertial frame, particle distance standard deviation (σ), and transmissivity (α) is given for each particle cluster at each time step. The particle

distance standard deviation (σ) describes how widely dispersed the particles in the cluster are. A value from 0 to 1 is given for the transmissivity of the particle, with 0 being opaque and 1 being transparent.

MATLAB was used to develop a script that post-processes the particle cluster output and converts it into a form more useful for assessing the severity of the brownout cloud generated by the helicopter. From the x, y, and z positions, the script builds a 3-dimensional grid around the aircraft, assigning a transmissivity value for each grid point. The 18.5 s time step, at which the aircraft is located 3 m above ground level (AGL) is typically when the brownout cloud is fully developed. Every particle cluster at this time step is mapped to the volumetric grid, with its corresponding transmissivity value assigned to each gridpoint within the standard deviation distance. Figure 3 depicts the particle cluster locations placed on the 3D grid for a UH-60 in a scenario with no wind.

While the transmissivity of each particle cluster at the given time step is provided in the output data, it must be recalculated based on the number of particles within each cluster and the standard deviation as the number of particles within the cluster volume is dependent on particle size. The transmissivity given in the output file assumes a fixed value for particle diameter, 20 μm, which is not applicable for these calculations. Every time the particle size is varied, the number of particles within each cluster will need to be recalculated using equation (9):

$$N_{part} = (N/Vol) \times Vol_{cluster} = (P_d/(\pi d^3/6)) \times (DX)(DY)(THICKNESS) \quad (9)$$

where P_d is the packing density of the material, d is the particle diameter, DX and DY are the $X-$ and $Y-$ extent of each particle cluster on the ground, and $THICKNESS$ is the vertical extent of the layer. The transmissivity of the particle

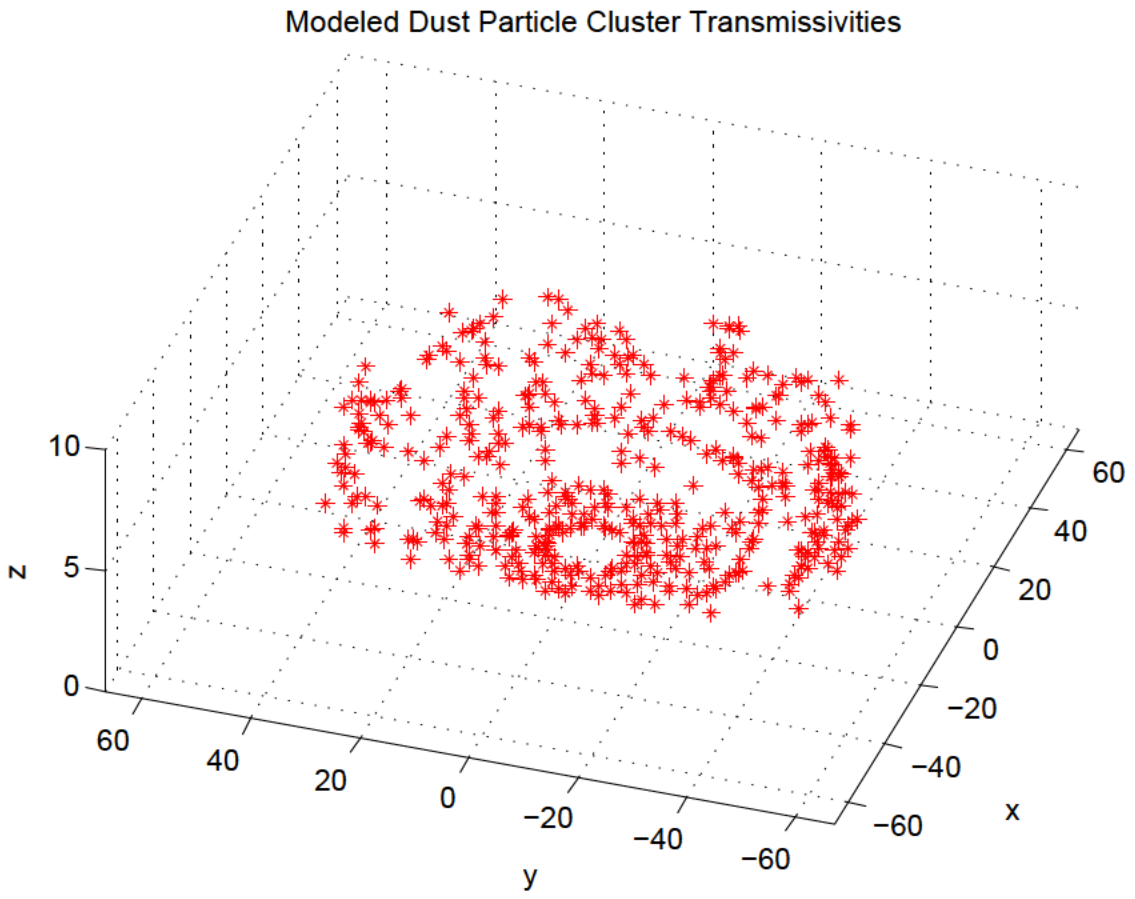

Figure 3. Modeled dust particle clusters mapped on volumetric grid about the landing point. Each red asterisk represents one dust particle cluster which contains thousands of dust particles. Shown in this figure are the locations of the clusters 18.5 seconds into the simulation run for a UH-60 with 10 micron particles and no atmospheric wind.

cluster can then be determined using equation (10):

$$\alpha = I/I_0 = e^{-\gamma\sigma} = exp(-\pi a^2 \rho Q \sigma) = exp(-\pi a^2 (N_{part}/(4/3)\pi\sigma^3) Q\sigma) \qquad (10)$$

where a is the particle radius, σ is the particle cluster distance standard deviation, and Q is the particle extinction efficiency factor. The particle extinction efficiency factor Q is set to 0.2 by CDI in the model code, which assumes a particle at the small end of the Mie scattering regime. This calculated transmissivity is the true

value for each particle cluster and will be used to find the transmissivity along a given line of sight. Each grid point may be affected by several particle clusters so the transmissivity values of the particle clusters affecting each grid point must be multiplied to determine the total transmissivity value for each grid point. Next, we integrate the transmissivities of all of the grid points along a linear path to obtain the transmissivity along a determined line of sight. Several trajectories were chosen for this study to obtain multiple viewpoints from within the brownout cloud.

Five trajectories were chosen for analysis: straight ahead, 90° right, 45° right, straight ahead and angled down 10°, and 45° right and angled down 10°. This assumes a nearly symmetric cloud so that trajectories directed to the right are nearly identical to trajectories to the left. For the lines of sight looking straight ahead and 90° right, cross sections are taken at 0.6 meters, 1.2 meters, 1.8 meters, 2.4 meters, and 3.0 meters above the ground and the line of sight looking 45° right is taken at 1.2 meters above the ground. The view geometry for the 0° or straight ahead line of sight can be seen in Figure 4.

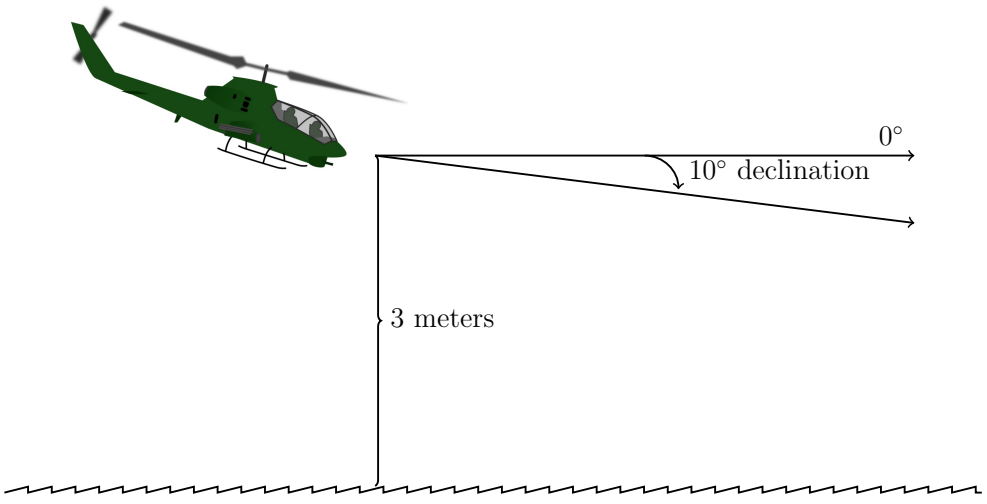

Figure 4. View geometry showing heading and declination angle.

3.3 Metric to Assess Brownout Severity of Particle Cloud

The transmissivity values calculated using the MATLAB post-processing script are useful, but require further information on visibility conversions and landing minimums in order to assess the severity of a given brownout cloud. One method of comparison is to compare these transmissivity values to the readings of transmissometer runway visual range (RVR) systems in use at airports with instrument runways. RVR is defined as the distance at which a pilot in an aircraft on the centerline of the runway can see the runway surface markings. It is used as one of the main criteria for minima on instrument approaches and landings and is usually given in feet or meters. Transmissometer systems measure a transmissivity alongside the runway, which can be equated to an RVR value. Table 3 from the USDC/NOAA Field Meteorological Handbook (2005) is a conversion table for comparing RVR to transmissivity values obtained from transmissometers during daylight.

Table 3. USDC/NOAA (2005) conversion from transmissivity to RVR for day.

RVR(m)	***Min***	***Max***
200	0.0449	0.0823
400	0.2905	0.3746
600	0.5107	0.5644
800	0.6499	0.6840
1000	0.7395	0.7774

The RVR distances are still not useful without knowledge of published instrumented landing and approach minimums. The Federal Aviation Agency mandates minimum runway criteria based on the type or category of flight operations an airfield can support. A ground facility is categorized based on its runway length, lighting system, and ground equipment. The minimum required RVR for landing and approach. In order to devise a practical brownout severity metric, transmissivity values corresponding to the Category II instrument landing system visibility minimum of 400

m will be considered moderate (amber) conditions. RVR values lower than 400 m will be classified as severe (red). The category I minimum of 800 m will be used as the threshold for low risk (green) conditions. According to the USDC/NOAA RVR to transmissivity conversions, 400 m RVR results from a transmissivity of 0.2905 to 0.3746 and 800 m RVR results from 0.6499 to 0.6840. For ease of delineating between green, amber, and red conditions, the average value for each RVR range was used. An RVR of 400 m would then have a corresponding transmissivity value of 0.3326 and an RVR of 800 m would have a transmissivity of 0.6670.

IV. Results and Analysis

This chapter presents the results obtained during this study. The first section compares each of the five different aircraft evaluated, the second section analyzes particle size impact on transmissivity, and the third section discusses the role of wind speed in the brownout clouds generated during the simulation runs. The last section examines the different lines of sight (LOS) used in post-processing the output data and their representativeness in characterizing the brownout cloud.

4.1 Aircraft Comparison

This section contains tables of all of the simulation and post-processing results broken down by aircraft. For each aircraft type there are transmissivities attained using 125 different combinations of particle size, wind speed, and LOS. Although post-processing produced 13 different lines of sight, only 5 were chosen to use for analysis as they were the most representative. The tables are presented in this section and will be referred to in the next few sections for further analysis. Table 4 catalogs the transmissivities obtained for all simulations run using the AH-64 aircraft.

For each particle size and wind speed combination tested, the AH-64 produced a significant brownout cloud. Transmissivities near zero were the norm. The 0° (straight ahead) LOS had the lowest transmissivity values, with the 90° (right-viewing) LOS close behind. Angled trajectories, whether horizontal at 45° or angled down from 3 meters off the ground, did not best depict the severity of the brownout cloud for this aircraft. In general, transmissivities decreased with increasing winds and increased with increasing particle sizes.

Table 5 contains results for the CH-47 simulations. Since this helicopter has a rotor configuration unlike any of the others evaluated, it was expected that the interactions

Table 4. Results from all AH-64 simulation runs after postprocessing output data

AH-64 Transmissivities		View Geometry				
Particle Size	**Wind Speed**	**Horiz Ahead**	**Horiz 45° Right**	**Horiz 90° Right**	**10°Down Ahead**	**10°Down 45°Right**
10 micron	**0 m/s**	0.0038	0.4124	0.0198	0.6841	0.7764
	3 m/s	0.0056	0.5231	0.1217	0.7233	0.8505
	6 m/s	0.0000	0.1432	0.0001	0.4449	0.2737
	9 m/s	0.0000	0.0749	0.0000	0.3784	0.2737
	12 m/s	0.0000	0.1683	0.0000	0.2737	0.6151
30 micron	**0 m/s**	0.2821	0.8098	0.4487	0.9587	0.8811
	3 m/s	0.1683	0.8976	0.4449	0.9474	0.9474
	6 m/s	0.0091	0.5521	0.0053	0.7634	0.7634
	9 m/s	0.0003	0.4449	0.0020	0.8057	0.5231
	12 m/s	0.0000	0.4215	0.0031	0.4696	0.3993
50 micron	**0 m/s**	0.3727	0.9269	0.6341	0.9750	0.9506
	3 m/s	0.2327	0.8785	0.4595	0.9681	0.9373
	6 m/s	0.0027	0.7471	0.3784	0.8785	0.7717
	9 m/s	0.0014	0.6779	0.1342	0.8233	0.6354
	12 m/s	0.0104	0.5581	0.2253	0.7971	0.5064
70 micron	**0 m/s**	0.5408	0.9821	0.6966	1.0000	0.9821
	3 m/s	0.1399	0.9329	0.6010	0.9548	0.9548
	6 m/s	0.1217	0.7233	0.3697	0.9329	0.7067
	9 m/s	0.0105	0.6010	0.2866	0.7402	0.6151
	12 m/s	0.0155	0.6906	0.2613	0.7753	0.9116
90 micron	**0 m/s**	0.5386	0.8811	0.5944	0.9860	0.9723
	3 m/s	0.1624	0.9646	0.7498	0.9646	0.9646
	6 m/s	0.0672	0.7914	0.6151	0.8816	0.7914
	9 m/s	0.0115	0.7233	0.2688	0.8976	0.7233
	12 m/s	0.0582	0.7498	0.4868	0.8353	0.6730

of the flow fields would create unique results. The CH-47 was the only aircraft that had lower transmissivity values for the 90° line of sight than it did for the 0° line of sight for most combinations of particle size and wind speed, most noticeably up to 50 μm. As with the AH-64, transmissivities decreased with increasing wind speed and increased with increasing particle size.

Table 6 contains results for the CH-53 simulations. Similar patterns existed with the CH-53 as with the previous aircraft; however it is interesting to note the contribu-

Table 5. Results from all CH-47 simulation runs after postprocessing output data

CH-47 Transmissivities		View Geometry				
Particle Size	**Wind Speed**	**Horiz Ahead**	**Horiz 45° Right**	**Horiz 90° Right**	**10°Down Ahead**	**10°Down 45°Right**
10 micron	**0 m/s**	0.0306	0.1865	0.0000	0.8788	0.5241
	3 m/s	0.0136	0.5161	0.0070	0.8476	0.7184
	6 m/s	0.0000	0.3142	0.0003	0.4374	0.5161
	9 m/s	0.0000	0.3707	0.0001	0.8476	0.8476
	12 m/s	0.0000	0.0510	0.0003	0.6089	0.8476
30 micron	**0 m/s**	0.4809	0.7086	0.0129	0.9175	0.8418
	3 m/s	0.1301	0.9464	0.0538	0.8476	1.0000
	6 m/s	0.3320	0.8476	0.2974	0.9464	0.8476
	9 m/s	0.0122	0.4140	0.0510	0.8476	0.6799
	12 m/s	0.0122	0.6434	0.1103	0.7591	1.0000
50 micron	**0 m/s**	0.2969	0.9018	0.2542	0.9745	0.9018
	3 m/s	0.3707	0.8476	0.2941	0.9055	0.9055
	6 m/s	0.1569	0.8476	0.2941	0.9675	1.0000
	9 m/s	0.0223	0.6294	0.0783	0.8200	0.8200
	12 m/s	0.0321	0.7675	0.0527	0.8761	1.0000
70 micron	**0 m/s**	0.6663	0.8163	0.2414	0.9817	0.9638
	3 m/s	0.3796	0.8886	0.2153	0.9098	0.9538
	6 m/s	0.2859	0.9098	0.6852	0.9538	0.9767
	9 m/s	0.0630	0.6536	0.5040	0.9316	0.9767
	12 m/s	0.0358	0.7184	0.0964	0.8678	0.9098
90 micron	**0 m/s**	0.7188	0.8418	0.3264	0.9857	0.9442
	3 m/s	0.1622	0.8793	0.3918	0.9464	0.9464
	6 m/s	0.1452	0.8956	0.5067	0.8321	0.9122
	9 m/s	0.0328	0.6925	0.1426	0.8476	1.0000
	12 m/s	0.0601	0.8956	0.2920	0.8633	0.9639

tion of the atmospheric winds in generating the brownout cloud. Since the CH-53 is by far the heaviest of the helicopters used in this study, it was expected that brownout cloud characteristics would reveal unique results based on the higher fluid threshold velocity this aircraft is capable of generating. The expectations were correct; as particle size increased, stronger winds were required to generate brownout clouds. Specifically, in windless conditions, particles larger than 30 μm did not generate a significant cloud.

Table 6. Results from all CH-53 simulation runs after postprocessing output data

CH-53 Transmissivities		View Geometry				
Particle Size	**Wind Speed**	**Horiz Ahead**	**Horiz 45° Right**	**Horiz 90° Right**	**10°Down Ahead**	**10°Down 45°Right**
10 micron	**0 m/s**	0.0107	0.4618	0.0060	0.8244	0.9079
	3 m/s	0.1223	0.7810	0.3287	0.8837	0.7810
	6 m/s	0.0000	0.0169	0.0000	0.1081	1.0000
	9 m/s	0.0000	0.0117	0.0000	0.4763	1.0000
	12 m/s	0.0000	0.0023	0.0000	1.0000	0.8837
30 micron	**0 m/s**	0.1816	0.4618	1.0000	0.8792	0.9079
	3 m/s	0.0515	0.6623	0.2269	0.8837	0.8138
	6 m/s	0.0035	0.9209	0.3425	0.7810	1.0000
	9 m/s	0.0000	0.3425	0.0001	0.8138	1.0000
	12 m/s	0.0000	0.0810	0.0001	0.8837	1.0000
50 micron	**0 m/s**	0.4708	0.9256	0.7063	0.9256	0.9809
	3 m/s	0.1285	0.8411	0.4533	0.9285	0.9285
	6 m/s	0.0025	0.5950	0.0364	0.6568	1.0000
	9 m/s	0.0001	0.4763	0.0502	1.0000	1.0000
	12 m/s	0.0000	0.2159	0.0030	1.0000	1.0000
70 micron	**0 m/s**	0.5229	0.9079	0.7801	0.9463	0.9863
	3 m/s	0.0800	0.9318	1.0000	0.8995	0.9318
	6 m/s	0.0349	0.7539	0.1594	0.8837	1.0000
	9 m/s	0.0031	0.4934	0.0362	0.8682	1.0000
	12 m/s	0.0013	0.4135	0.0109	1.0000	1.0000
90 micron	**0 m/s**	0.5785	0.9177	0.7565	0.9683	0.9893
	3 m/s	0.2826	0.8251	0.8717	0.9596	0.9336
	6 m/s	0.0095	0.7703	0.2061	0.8480	0.9729
	9 m/s	0.0096	0.6443	0.2032	0.9864	1.0000
	12 m/s	0.0070	0.4963	0.0407	0.9864	1.0000

Table 7 includes the results acquired from the UH-1H simulations. This aircraft is at the opposite end of the weight spectrum from the CH-53 and is the lightest of the helicopters chosen for this study. The lighter mass significantly suppressed brownout cloud generation, as this aircraft barely lofted enough particles to create a dust cloud. The only significant combinations were particle diameter of 10 μm and wind speed of 9 m s^{-1} or greater.

Table 8 includes the transmissivities obtained during the UH-60 simulations. The

Table 7. Results from all UH-1H simulation runs after postprocessing output data

UH-1H Transmissivities		**View Geometry**				
Particle Size	**Wind Speed**	**Horiz Ahead**	**Horiz 45° Right**	**Horiz 90° Right**	**10°Down Ahead**	**10°Down 45°Right**
10 micron	**0 m/s**	1.0000	0.7688	0.7688	0.5910	1.0000
	3 m/s	1.0000	1.0000	0.5101	1.0000	0.7142
	6 m/s	0.5101	1.0000	0.7142	0.7142	0.7142
	9 m/s	0.3643	1.0000	0.1858	0.3643	1.0000
	12 m/s	0.2602	1.0000	0.5101	1.0000	0.7142
30 micron	**0 m/s**	0.9161	1.0000	0.9161	1.0000	0.9161
	3 m/s	0.8939	1.0000	0.7990	1.0000	1.0000
	6 m/s	0.7990	1.0000	1.0000	0.8939	0.8939
	9 m/s	0.7990	0.8939	0.8939	0.7990	0.8939
	12 m/s	0.4559	0.8939	0.7142	0.7990	0.7990
50 micron	**0 m/s**	0.9488	1.0000	0.9002	0.9002	0.9002
	3 m/s	0.8171	1.0000	0.8171	0.8740	1.0000
	6 m/s	0.9349	0.9349	0.9349	0.9349	1.0000
	9 m/s	0.9349	1.0000	0.9349	0.8740	1.0000
	12 m/s	0.7639	0.9349	0.8171	0.8740	1.0000
70 micron	**0 m/s**	1.0000	1.0000	1.0000	1.0000	1.0000
	3 m/s	0.8250	1.0000	0.9083	1.0000	1.0000
	6 m/s	0.7494	1.0000	1.0000	0.9531	0.9083
	9 m/s	0.9531	0.9531	0.9531	0.9083	0.9531
	12 m/s	0.8250	0.9083	0.8657	0.9083	0.9531
90 micron	**0 m/s**	0.9712	1.0000	1.0000	0.9712	1.0000
	3 m/s	0.8939	0.9633	1.0000	0.9633	1.0000
	6 m/s	0.7142	1.0000	1.0000	0.9279	0.7990
	9 m/s	0.8610	1.0000	0.8610	1.0000	1.0000
	12 m/s	0.7414	0.9633	0.8610	0.9279	0.9633

UH-60 had the most consistent results of the aircraft tested. In general, transmissivities decreased with increasing wind speed and increased with increasing particle size. The 0° and 90° lines of sight both revealed a significant brownout cloud generated for most combinations of wind speed and particle size.

Overall, every aircraft type produced results that were consistent with expectations. Each helicopter interacted uniquely with the atmospheric head wind, creating different results for every wind speed and particle size pairing. The next few sections

Table 8. Results from all UH-60 simulation runs after postprocessing output data

UH-60 Transmissivities		View Geometry				
Particle Size	**Wind Speed**	**Horiz Ahead**	**Horiz 45° Right**	**Horiz 90° Right**	**10°Down Ahead**	**10°Down 45°Right**
10 micron	**0 m/s**	0.0129	0.8561	0.0522	0.7328	0.8561
	3 m/s	0.0003	0.3699	0.0008	0.8196	1.0000
	6 m/s	0.0000	0.2484	0.0005	0.5506	0.8196
	9 m/s	0.0000	0.1121	0.0017	0.2484	0.3699
	12 m/s	0.0000	0.2036	0.0000	0.2484	0.4513
30 micron	**0 m/s**	0.2739	0.8128	0.2600	0.9495	0.9016
	3 m/s	0.0982	0.8196	0.4822	0.9358	0.9358
	6 m/s	0.0279	0.6287	0.0506	0.8196	1.0000
	9 m/s	0.0006	0.5152	0.0388	0.6718	0.7178
	12 m/s	0.0000	0.3699	0.0126	0.6287	0.8196
50 micron	**0 m/s**	0.4188	0.9397	0.2249	0.9694	1.0000
	3 m/s	0.1541	0.9610	0.3849	0.9610	0.9235
	6 m/s	0.1077	0.8529	0.4513	0.8875	0.9235
	9 m/s	0.0061	0.6990	0.4337	0.6990	0.8196
	12 m/s	0.0187	0.4696	0.1263	0.8529	0.8875
70 micron	**0 m/s**	0.5137	0.9150	0.5614	0.9780	0.9780
	3 m/s	0.1717	0.8196	0.8432	0.9720	0.9720
	6 m/s	0.0222	0.8925	0.3396	0.8196	0.9447
	9 m/s	0.0478	0.7315	0.4914	0.8196	0.7966
	12 m/s	0.0775	0.7315	0.3301	0.8925	1.0000
90 micron	**0 m/s**	0.7718	0.9333	0.6061	1.0000	1.0000
	3 m/s	0.3952	0.9781	0.7178	1.0000	1.0000
	6 m/s	0.1948	0.8567	0.3312	0.9154	0.8379
	9 m/s	0.1823	0.8379	0.4223	0.9358	0.8379
	12 m/s	0.0443	0.7503	0.3781	0.8567	0.9358

will analyze particle size and wind speed impact on brownout cloud generation and evolution.

4.2 Particle Size Comparison

As particle size increases, the dust cloud becomes more transparent. Dust particle mass increases with the cube of its radius, while its cross-sectional area only increases with the square of its radius. Thus, the ability of the rotorwash to pick up dust

particles falls off more rapidly with increasing particle size than does the particles' optical effects. It would be expected then that the following plots of cluster transparencies from a horizontal slice 1.5 meters above the ground would depict increasing transparencies with increasing particle diameters, consistent with observations from the previous section. The locations of the particle clusters on the grid are not necessarily intuitive, however. Two aircraft, the UH-60 and the CH-47, were chosen for these plots in order to show the difference between the aerodynamic influences of a traditional main and tail rotor system and that of a twin rotor system. The UH-60 was chosen over the other helicopters with a main and tail rotor system because its mass is the median of the masses of the aircraft being assessed and should therefore give the most representative results.

Figure 5 depicts CH-47 transmissivities with no atmospheric wind and particle sizes ranging from 10 μm to 70 μm. As expected, the plots show increasing transparency with increasing particle diameter. It is interesting to note that as particle diameter increases, the clusters are pushed further outward. The 50 μm plot, however, shows an arc of space that is void of particle clusters with a pile up close to the landing point and a scattering of clusters on the periphery. The 70 μm plot follows the pattern of the 10 μm and 30 μm plots; more clusters pushed radially outward as diameter increases. The aerodynamic influence of the CH-47's twin rotor system causes the particle clusters to take on a different configuration than a more traditional main and tail rotor system. Particle clusters are pushed away from the nose of the CH-47, creating more of a bow or semi-circle.

Figure 6 shows the same plots for a UH-60 with no atmospheric wind. The UH-60, having a four-blade main and tail rotor system, tends to push particles out radially from the aircraft. As with the CH-47, particle clusters with larger particle diameters are pushed further outward, but in this case, in a more radially symmetrical pattern.

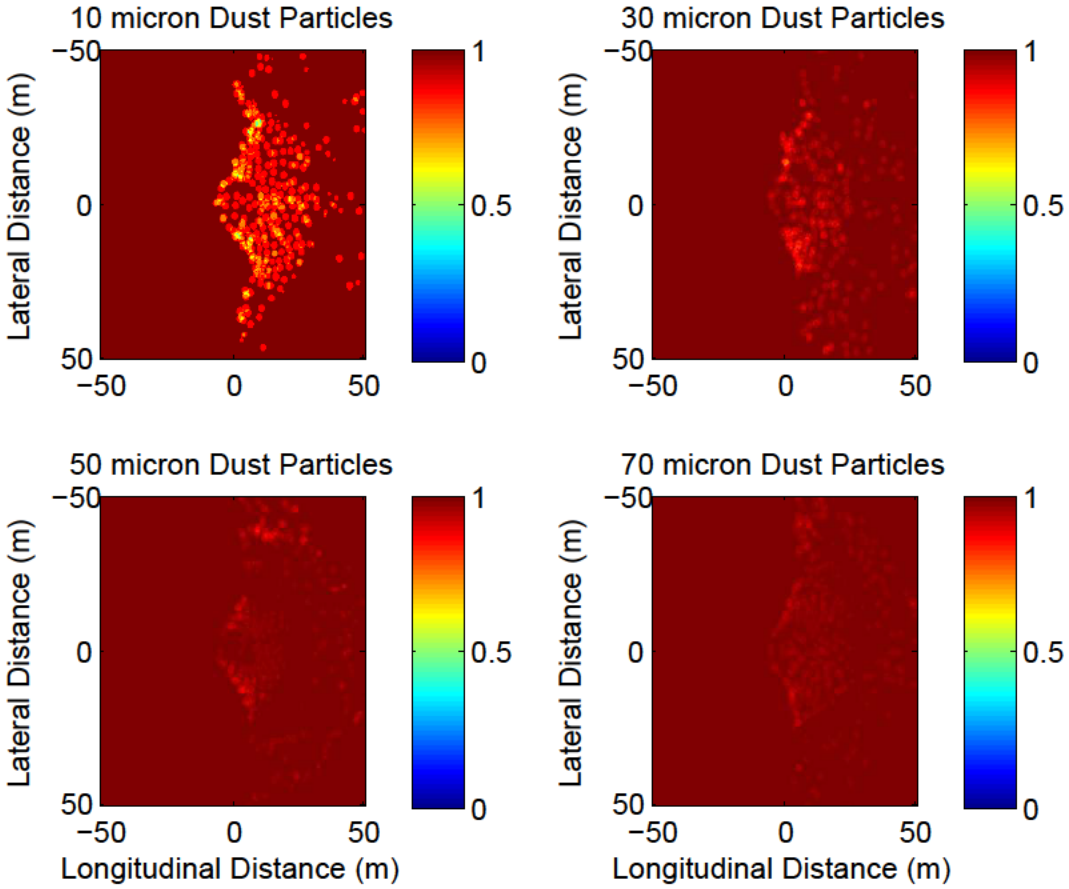

Figure 5. Modeled dust particle clusters for a CH-47 simulation run with no atmpspheric wind. Each subplot shows the particle cluster locations and transmissivities at 18.5 seconds into the simulation run for the particle diameter specified.

The arc void of particle clusters that was observed in the plots for the CH-47 at 50 μm is now seen at both 30 μm and 50 μm for the UH-60. A circle of particle clusters exists around the landing point, then there is a gap before the clusters emerge again on the outskirts of the cross section.

While the first two quad plots did not include the effects of wind, the next two figures depict results for the same two aircraft but with the influence of a headwind of 6 m s^{-1}. Figure 7 depicts the cluster transparencies and locations for a CH-47 with 6 m s^{-1} of atmospheric wind coming from head on (right-hand side of the plot). The interaction of the headwind and the twin rotor system appears to result in a

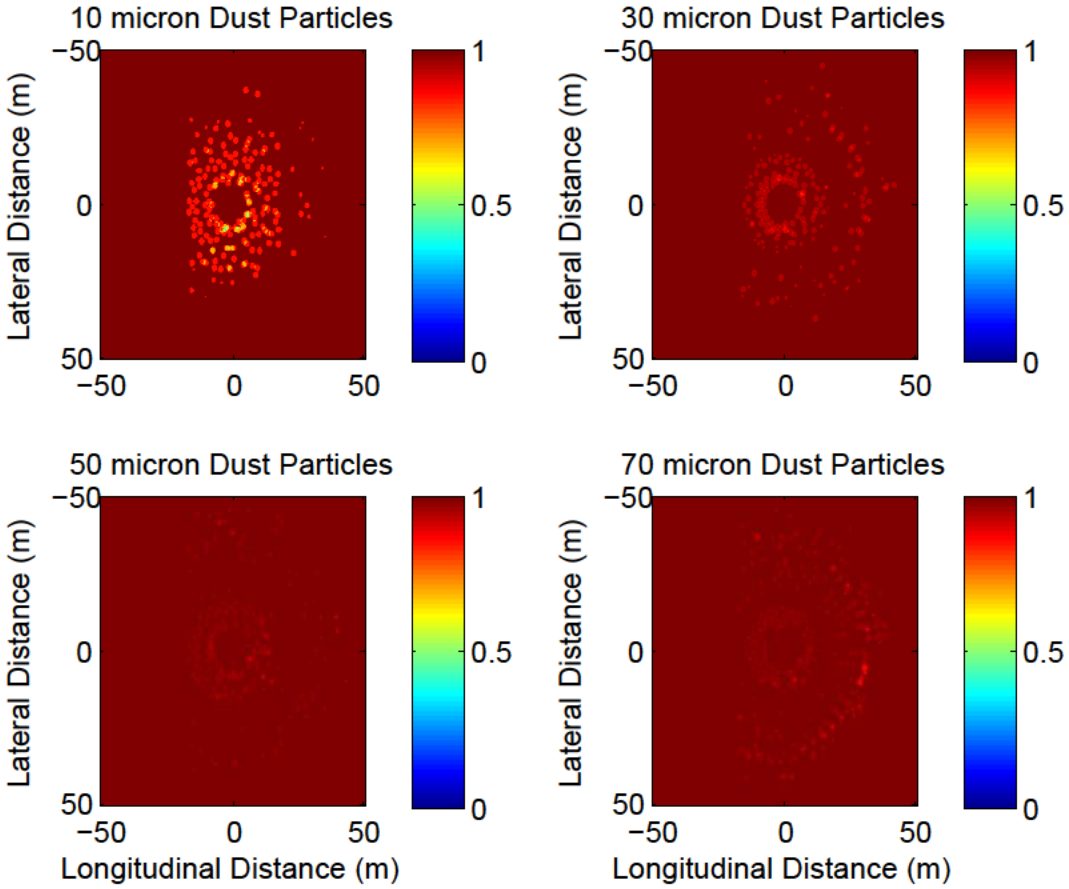

Figure 6. Modeled dust particle clusters for a UH-60 simulation run with no atmpspheric wind. Each subplot shows the particle cluster locations and transmissivities at 18.5 seconds into the simulation run for the particle diameter specified.

breakdown of the expected pattern.

The particle clusters are much more scattered, but are not necessarily dispersed radially outward. The twin rotor system is very visible on the 30 μm subplot with large gaps where the rotors are pushing particles away. The 50 μm subplot shows more of a semi-circle or arc, as before, but in this case no gap in clusters exists. The most interesting plots, however, are the 10 μm and 70 μm subplots, where the headwind interaction with the twin rotor systems is very apparent. The rotor downwash meets with the headwind approximately even with the tail of the aircraft, creating a line of clusters at $x = 0$ with a less defined arc of particles ahead of the aircraft.

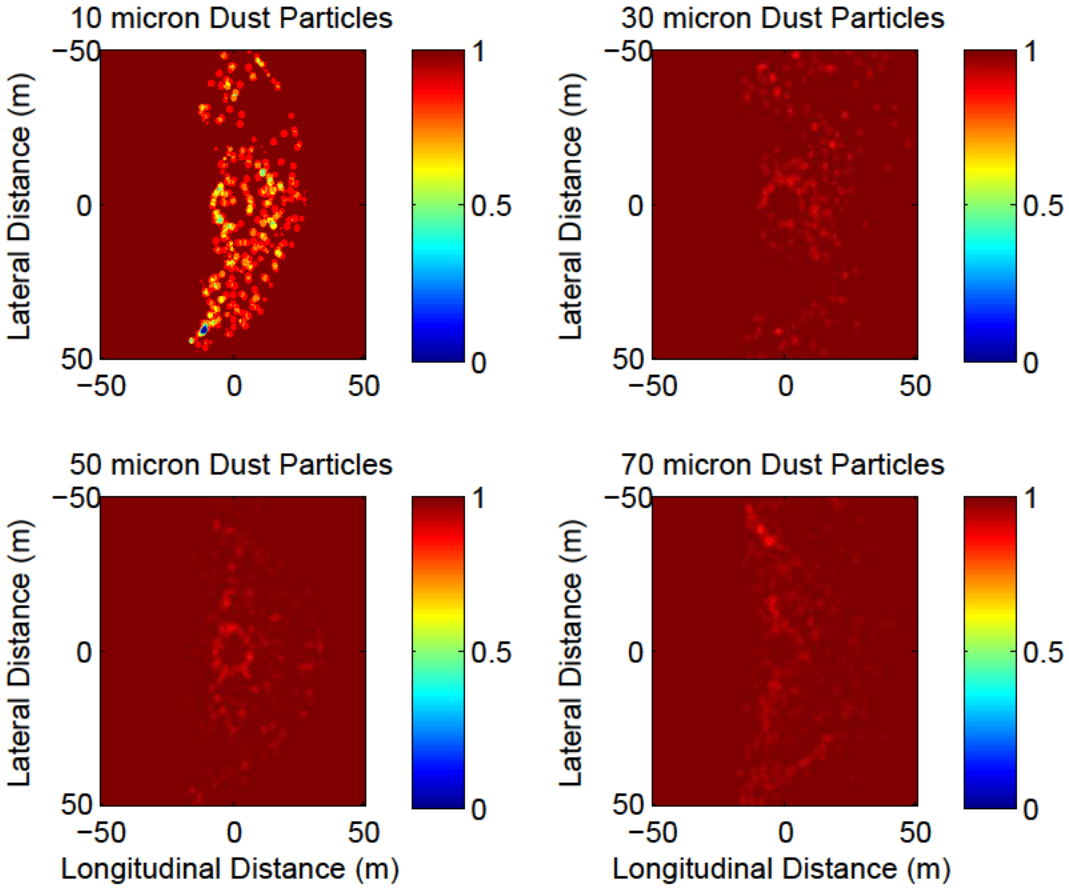

Figure 7. Modeled dust particle clusters for a CH-47 simulation run with a 6 m s^{-1} headwind. Each subplot shows the particle cluster locations and transmissivities at 18.5 seconds into the simulation run for the particle diameter specified.

Figure 8 shows UH-60 results with a 6 m s^{-1} headwind. A similar wall of particle clusters is observed in these plots, most distinctly for the 30 μm through 70 μm particle diameters. The interesting aspect of these plots is the location of the edge of the clusters, or the point where the rotor downwash meets the headwind. This edge occurs nearly 15 m behind the aircraft.

The plots for the CH-47 and UH-60 depict considerably different particle configurations for each wind speed evaluated. The UH-60 tended to have a more annular grouping of clusters surrounding the landing point, while the CH-47 had more of a crescent shape. These particle cluster configurations shed some light on the differ-

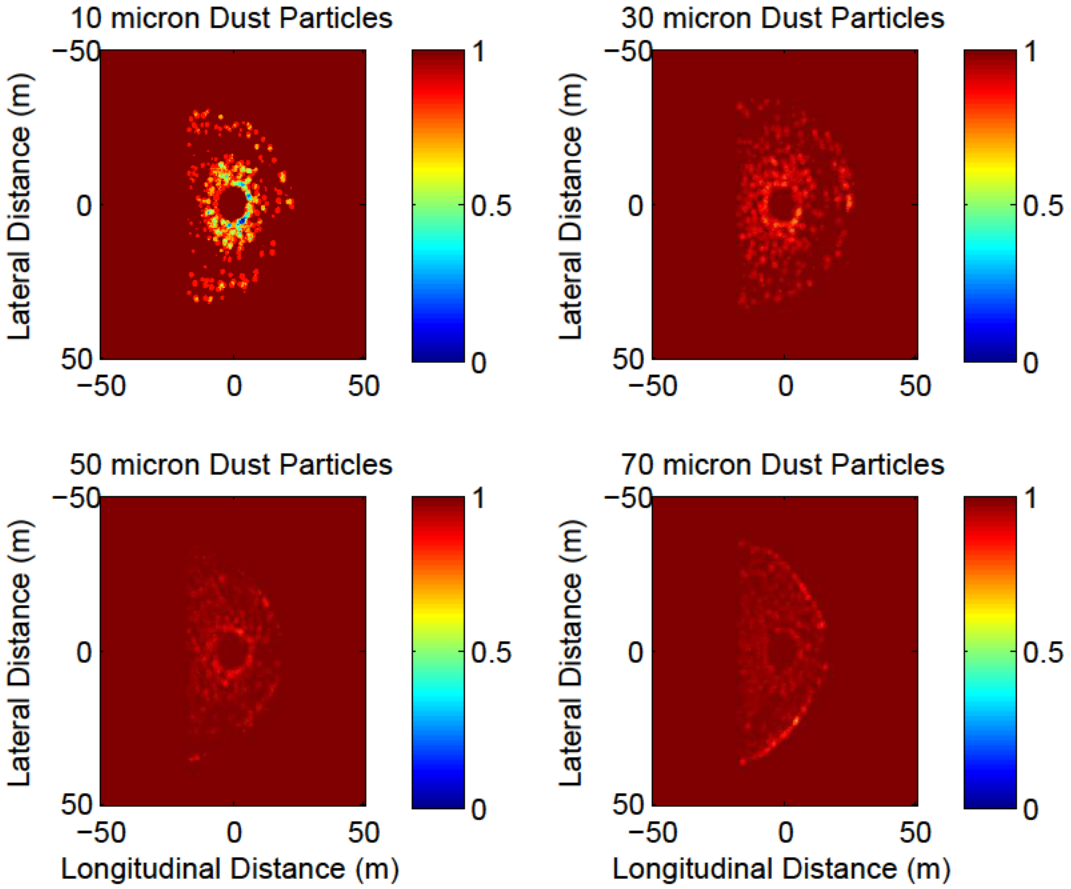

Figure 8. Modeled dust particle clusters for a UH-60 simulation run with a 6 m s^{-1} headwind. Each subplot shows the particle cluster locations and transmissivities at 18.5 seconds into the simulation run for the particle diameter specified.

ences observed in transmissivity values for the same LOS between different aircraft types. The UH-60 had the largest aggregation of clusters in front of the aircraft, while the CH-47 tended to aggregate clusters both in front of and to the side of the aircraft. When an atmospheric headwind of 6 m s^{-1} was added, the particle clusters generally formed a convergence line where the rotor downwash met the atmospheric wind.

4.3 Wind Speed Comparison

The following figures depict transmissivity vs. wind speed computed along the 0° LOS for the specified combinations of particle size and wind speed for each aircraft type. They are intended to depict trends and show the impact of different wind speeds on the calculated transmissivities for each particle diameter investigated.

Figure 9 shows the results of the AH-64 simulations. The 10 μm particle size had transmissivities of nearly zero for each wind speed, while the other particle sizes exhibited a decreasing trend in transmissivities with increasing wind speed, as discussed in the first section of this chapter. Some data points in this figure do not follow the trend though. Both the 70 μm particle diameter with a 6 m s^{-1} head wind and the 90 μm particle size with a 12 m s^{-1} head wind produce higher transmissivities (more transparent) than would be expected fromthe trend of the other combinations. Above 6 m s^{-1}, all particle sizes result in transmissivities of less than 0.1 for the AH-64.

Figure 10 shows the results and plots transmissivity trends for the simulation runs using the CH-47 and the 0° line of sight. Once again the 10 μm particle size results in near zero transmissivities for all wind speeds. In general there is a decreasing trend of transmissivities with increasing wind speed, but there are a few interesting exceptions. At 6 m s^{-1}, the 30 μm dust particle shows a sharp and unexpected increase in transmissivity, more than 0.2 above where the trend would place it. The 50 μm particle size with a 3 m s^{-1} head wind results in a transmissivity of approximately 0.07, larger than the same particle size without a head wind.

Figure 11 depicts the results from the CH-53 simulations. The 10 μm particle size does not follow the trend in this case, with a higher than expected transmissivity when paired with a 3 m s^{-1} atmospheric headwind. The rest of the results fall in line with trends, showing an appropriate decrease in transmissivity with increasing headwind for all other particle sizes. At and above 6 m s^{-1}, all particle sizes show

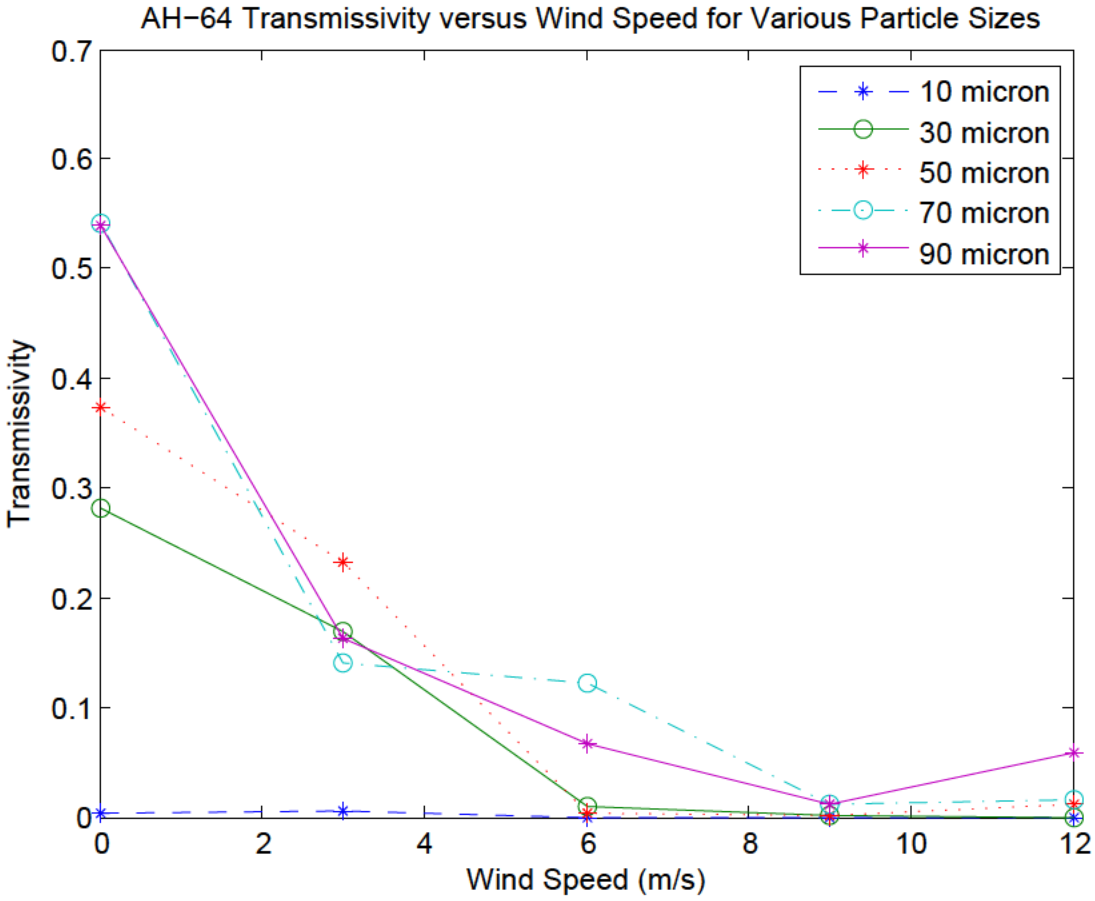

Figure 9. AH-64 transmissivity vs. wind speed for various particle sizes at 0° line of sight.

a trend of transmissivities converging to zero. Without a headwind, only the 10 μm and 30 μm diameter particles are able to be lifted enough to generate a significant dust cloud.

Figure 12 shows results for the UH-1H. As previously discussed, the UH-1H did not appear to produce a significant brownout cloud in these simulations, as transmissivities were nearly 1 for most cases. Since the UH-1H is such a light aircraft, it appears to have a difficult time entraining dust particles in its flow field. Only the 10 μm particle size was able to be lifted enough to show any noticeable decrease in transmissivity, and only when the head wind was at its strongest. The 30 μm particle

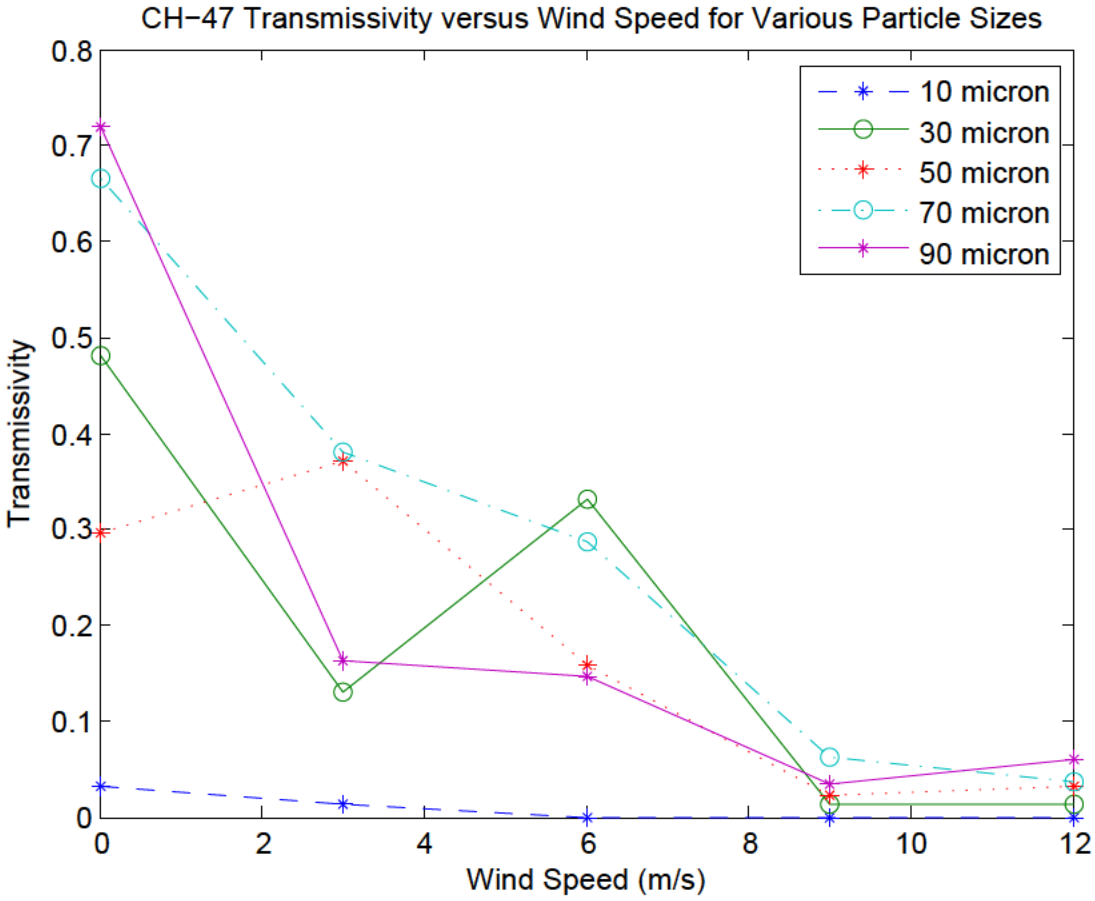

Figure 10. CH-47 transmissivity vs. wind speed for various particle sizes at 0° line of sight.

was able to be lifted with a 12 m s^{-1} headwind but the transmissivity only dropped to 0.45, still relatively transparent compared with other results.

Figure 13 shows results for the UH-60 helicopter. Nearly all particle size and wind speed combinations produce results consistent with trends, with the exception of the 70 μm particle size. When the headwind is increased above 6 m s^{-1}, transmissivity gradually improves by a small amount. Aside from that one anomaly, this aircraft produced the most consistent results for the 0° LOS. Transmissivity decreased as wind speed increased for every particle size and as particle size increased, so did transmissivity with each atmospheric wind speed tested.

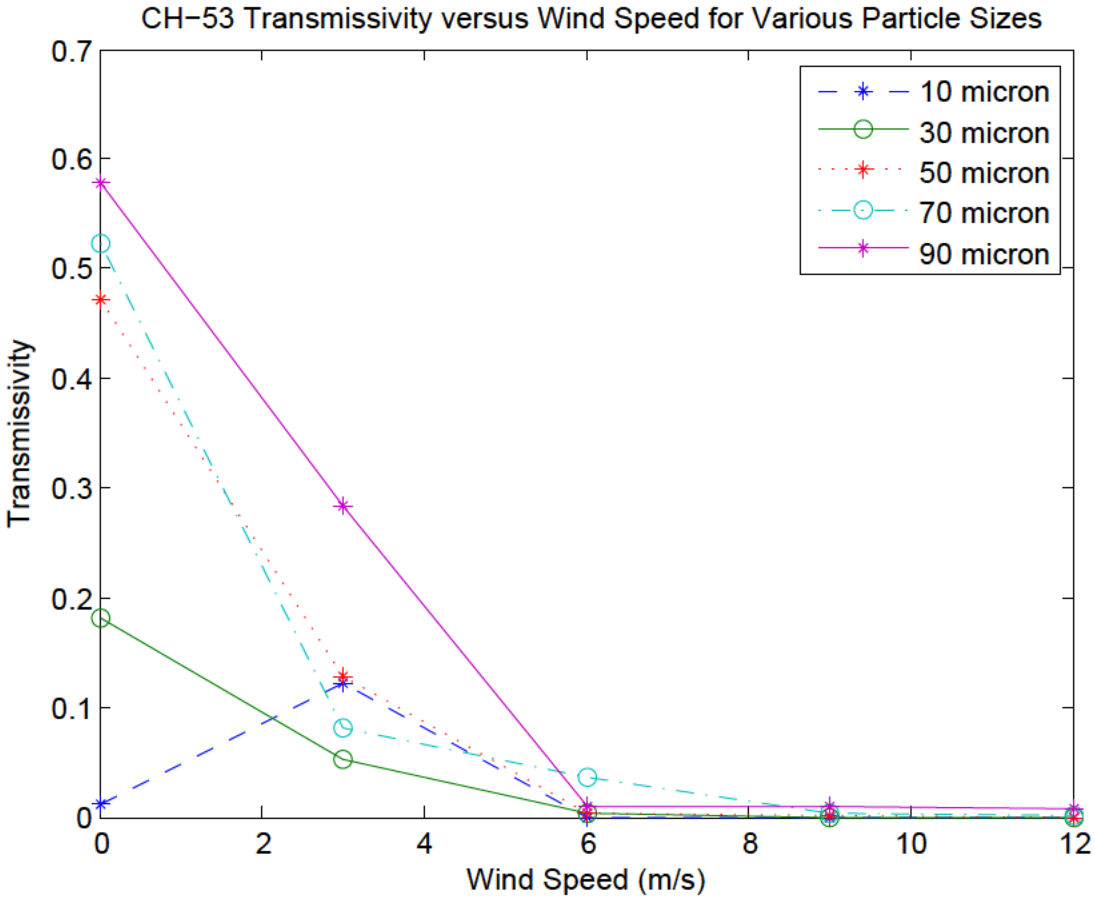

Figure 11. CH-53 transmissivity vs. wind speed for various particle sizes at 0° line of sight.

For each aircraft type, the overall trend was decreasing transmissivity with increasing wind speed, with a few exceptions. The UH-1H was unable to achieve a significant brownout cloud due to its light mass. The UH-60 produced the most consistent results, and due to its mid-range mass, it would likely be the most representative aircraft if only one type of helicopter was to be chosen for development of a brownout forecast algorithm.

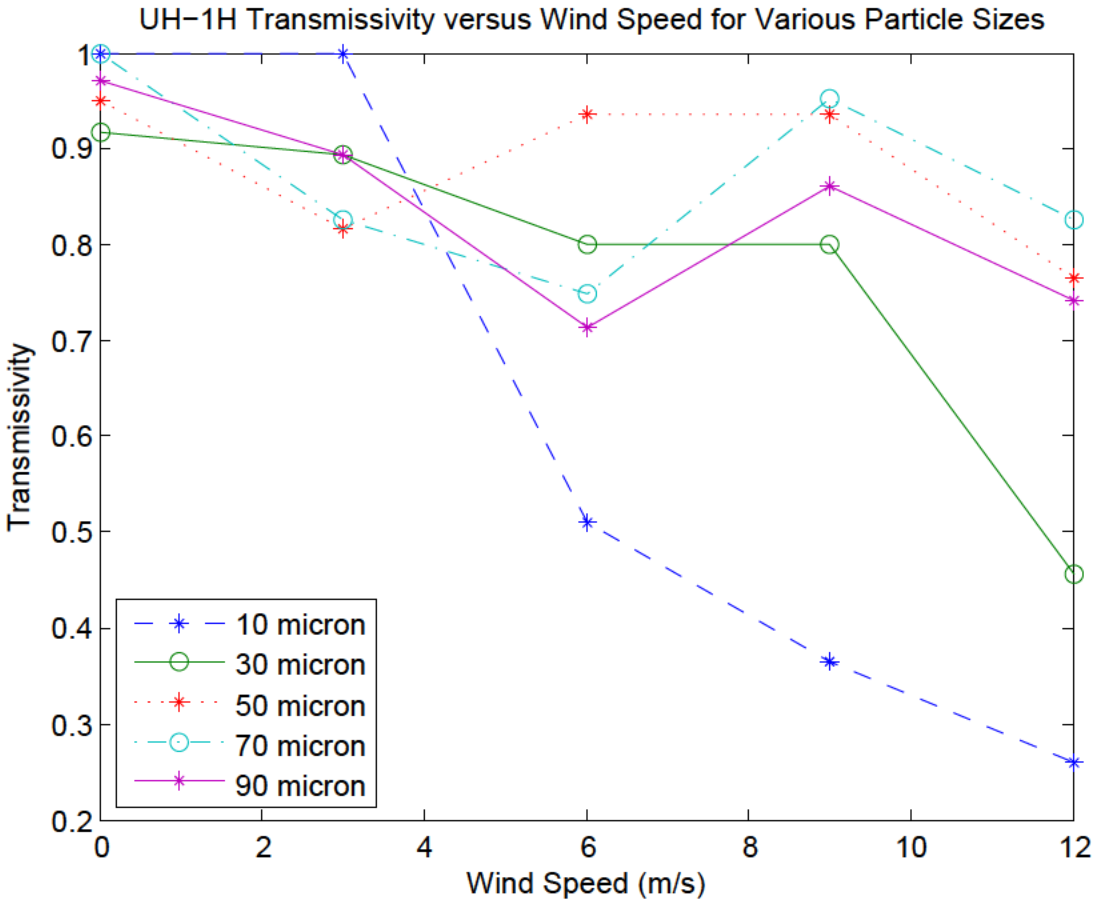

Figure 12. UH-1H transmissivity vs. wind speed for various particle sizes at 0° line of sight.

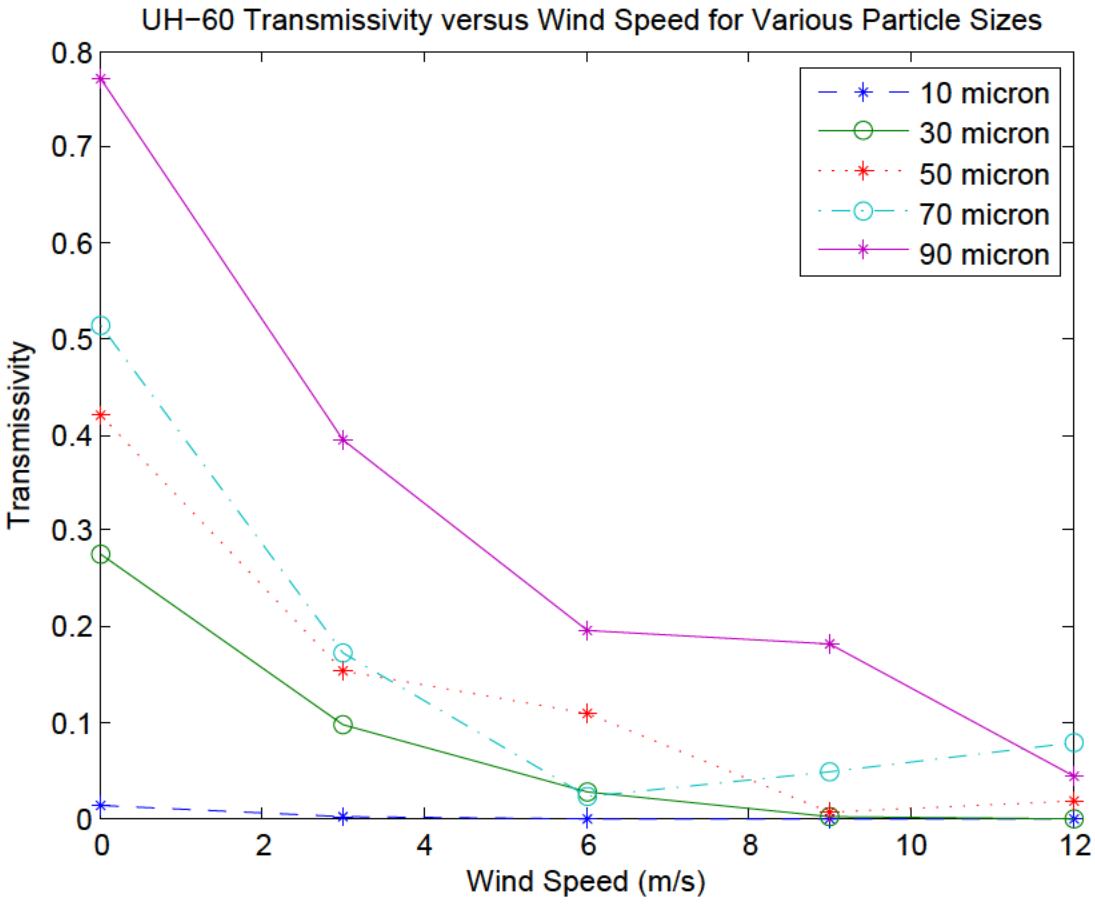

Figure 13. UH-60 transmissivity vs. wind speed for various particle sizes at 0° line of sight.

V. Conclusions

This chapter provides a summary of the study and the results found and concludes with additional comments regarding future research.

5.1 Summary of Results

The objective of this study was to investigate the effect of particle size and wind speed on brownout cloud generation and evolution for a variety of different rotary-wing aircraft types. To accomplish this task, 125 simulations were run, each with a different combination of aircraft type, particle size, and wind speed, using the Brownout Simulation and Analysis Model developed by Continuum Dynamics, Inc. Output characterizing the brownout cloud generated during each simulation was then post-processed to convert particle cluster information to transmissivity values for specified lines of sight.

The post-processing script read particle cluster positions, particle cluster standard deviation, and particle size for a single time step in the simulation and used those variables to calculate particle cluster volume and transmissivity. The clusters and their respective transmissivities were then mapped to a volumetric grid and each grid point was assigned a transmissivity value based on the particle clusters affecting that grid point. In order to obtain a transmissivity for each line of sight, the transmissivities of each grid point along theline of sight were integrated. Transmissivities were converted to runway visual range (RVR) values using a NOAA conversion chart, then compared to FAA instrument approach minimums to determine a metric quantifying pilot visibility obscuration due to the brownout cloud.

The Category II ILS visibilty minimum of 400 m was used as the threshold for severe brownout conditions (shaded red in Table 9) and the Category I minimum of

Table 9. Results from all simulations for the 0° line of sight. Transmissivities from 0 to 0.3326 (RVR of approximately 400 m) are shaded red, 0.3326 to 0.6670 (RVR of approximately 800 m) are shaded amber, and above 0.6670 are shaded green.

Particle Size	Wind Speed	AH-64 Results	CH-47 Results	CH-53 Results	UH-1H Results	UH-60 Results
10 μm	0 m/s	0.0038	0.0306	0.0107	1.0000	0.0129
	3 m/s	0.0056	0.0136	0.1223	1.0000	0.0003
	6 m/s	0.0000	0.0000	0.0000	0.5101	0.0000
	9 m/s	0.0000	0.0000	0.0000	0.3643	0.0000
	12 m/s	0.0000	0.0000	0.0000	0.2602	0.0000
30 μm	0 m/s	0.4809	0.1816	0.9161	0.2739	0.8811
	3 m/s	0.1683	0.1301	0.0515	0.8939	0.0982
	6 m/s	0.0091	0.3320	0.0035	0.7990	0.0279
	9 m/s	0.0003	0.0122	0.0000	0.7990	0.0006
	12 m/s	0.0000	0.0122	0.0000	0.4559	0.0000
50 μm	0 m/s	0.2969	0.4708	0.9448	0.4188	0.9506
	3 m/s	0.2327	0.3707	0.1285	0.8171	0.1541
	6 m/s	0.0027	0.1569	0.0025	0.9349	0.1077
	9 m/s	0.0014	0.0223	0.0001	0.9349	0.0061
	12 m/s	0.0104	0.0321	0.0000	0.7639	0.0187
70 μm	0 m/s	0.6663	0.5229	1.0000	0.5137	0.9821
	3 m/s	0.1399	0.3796	0.0800	0.8250	0.1717
	6 m/s	0.1217	0.2859	0.0349	0.7494	0.0222
	9 m/s	0.0105	0.0630	0.0031	0.9531	0.0478
	12 m/s	0.0155	0.0358	0.0013	0.8250	0.0775
90 μm	0 m/s	0.7188	0.5785	0.9712	0.7718	0.9723
	3 m/s	0.1624	0.1622	0.2826	0.8939	0.3952
	6 m/s	0.0672	0.1452	0.0095	0.7142	0.1948
	9 m/s	0.0115	0.0328	0.0096	0.8610	0.1823
	12 m/s	0.0582	0.0601	0.0070	0.7414	0.0443

800 m was used as the threshold for moderate brownout conitions (shaded amber in Table 9). An RVR of 400 m was assumed to correspond to a transmissivity value of 0.3326 and an RVR of 800 m to a transmissivity value of 0.6670.

Results for the five different rotary aircraft types, five particle sizes, and five wind speeds were presented and analyzed. The 0° line of sight provided the most consistent and reliable results for each aircraft investigated, so it was used for the final comparison. Table 9 presents the results for all five aircraft types, five wind speeds,

and five particle sizes for the 0° line of sight, color coded based on brownout severity. A significant majority of the cases produced severe brownout, which was somewhat expected due to the particle sizes and wind direction chosen. The headwind pushes the dust particle clusters back into the rotar downwash where the convergence of the headwind and downwash amplified the existing brownout cloud.

5.2 Future Work

Future research should combine these results with numerical weather prediction (NWP) output by developing an algorithm that includes the effects of dust particle size and forecasted wind speed to create a brownout prediction tool that maps the likelihood of brownout over a specified region. While five different aircraft types were evaluated in this study, choosing just one aircraft type may be more practical for such an algorithm. In that case, the UH-60 would be the most representative aircraft to choose.

Since these results only account for a headwind, it would be worthwhile to investigate the effects of wind from other directions. An atmospheric wind that either side of the aircraft may act to push the brownout cloud out from around the helicopter or it may cause other lines of sight have lower transmissivity values than the 0° viewing angle. Another variable of interest in modeling brownout is soil moisture which has a direct impact on a soil's lofting potential. While this study varied particle size, there was no way to adjust the moisture content of the soil itself within the model. As discussed in chapter II, soil moisture also further complicates the equations used to determine threshold velocity, as water acts as a binding agent between soil particles. This parameter is especially useful in numerical weather prediction, but is difficult to measure in situ. Future research should include an examination of soil moisture impact on brownout cloud generation and evolution. Finally, as discussed in section

3.2, the particle extinction efficiency factor Q was set to 0.2 in the CDI model and remained fixed for every particle size tested. Future work could also include studies of the effects of varying the extinction efficiency to reflect actual Q values consistent with the dust particle size simulated.

References

Allen, D.J., Kasibhatla, P., Thompson, A.M., Rood, R.B., Doddridge, B.G., Pickering, K.E., Hudson, R.D., Lin, S., 1996: Transport-induced interannual variability of carbon monoxide determined using a chemistry and transport model. *Journal of Geophysical Research*, Vol. 101, No. D22, pp 655-669.

Bacon, S. N., McDonald, E. V., Amit, R., Enzel, Y., and Crouvi, O., 2011: Total suspended particulate matter emissions at high friction velocities from desert landforms. *Journal of Geophysical Research*, Vol. 116, pp 1-17.

Bagnold, R.A., 1954: The Physics of Blown Sand and Desert Dunes, Methuen and Co. Ltd.

Chin, M., Rood, R.B, Lin, S., Muller, J., Thompson, A.M., 2000: Atmospheric sulfur cycle simulated in the global model GOCART: Model description and global properties. *Journal of Geophysical Research*, Vol. 105, No. D20, pp 671-687.

Cowherd, C., 2007: Sandblaster 2 Support of See-Through Technologies for Particulate Brownout - Task 5 Final Technical Report. Midwest Research Institute, MRI Project No. 110565 under DARPA Contract No. W31P4Q-07-C-0215.

Fecan, F., Marticorena, B., and Bergametti, G., 1999: Parameterization of the increase of the aeolian erosion threshold wind friction velocity due to soil moisture for arod and semi-arid areas. *Annales Geophysicae*, Vol. 17, pp 149-157.

Ghosh, S., Lohry, M.W., Rajagopalan, R. G., 2010: Rotor configuration effect on rotorcraft brownout. Presented at 2010 AIAA Applied Aerodynamics Conference, Chicago, IL.

Gillette, D. A., 1974: On the production of soil wind erosion aerosols having the potential for long-term transport. *Journal of Atmospheric Research*, Vol. 8, pp 735-744.

Ginoux, P., Chin, M., Tegen, I., Prospero, J. M., Holben, B., Dubovik, O., and Lin, S., 2001: Sources and distributions of dust aerosols simulated with the GOCART model. *Journal of Geophysical Research*, Vol. 106, No. 20, pp 255-273.

Haehnel, R., Buck, N., Song, A., 2013: Moisture effects on eolian particle entrainment. *Environmental Fluid Mechanics*.

Hillel, D., 2004: *Introduction to Environmental Soil Physics*, Academic Press.

Holton, J.R., 2004: *An Introduction to Dynamic Meteorology, Fourth Edition*, Elsevier Academic Press.

IPCC (Intergovernmental Panel on Climate Change), 2007: *Summary for policymakers*, Climate Change 2007: Impacts, Adaptation and Vulnerability. Contribution of Working Group II to the Fourth Assessment Report of the Intergovernmental Panel on Climate Change, Chambridge Univ. Press, pp7-22.

Iverson, J.D., Pollack, J.B., Greeley, R., and White, B.R., 1976: Saltation threshold on Mars: The effect of inter-particle force, surface roughness and low atmospheric density. *Icarus*, Vol. 29, pp 381-393.

Jones, S., 2012: Technical report on dust source region parameterization research. Prepared under contract no. FA4600-08-D-0002, Northrup Grumman Information Systems.

Kok, J.F., Parteli, E.J., Michaels, T.I., Karam, D.B., 2012: The physics of windblown sand and dust. *Rep. Prog. Phys.*, Vol. 75.

Lary, D. J., and Walker, A. L., 2011: High resolution identification of dust sources using machine learning and remote sensing data. *Presented at the American Geophysical Union 2011 Fall Meeting, San Francisco, California.*

Lu, H., and Shao, Y., 2001: Toward quantitative prediction of dust storms: An integrated wind modelling system and its applications. *Environmental Modelling and Software*, Vol. 16, No. 3, pp 233-249.

Macpherson, T., Nickling, W. G., Gillies, J. A., and Etyemezian, V., 2008: Dust emissions from undisturbed and disturbed supply limited desert surfaces. *Journal of Geophysical Research*, Vol. 113.

Marek, S.L., 2009: A computational tool for evaluating THz imaging performance in brownout conditions at land sites throughout the world. MS thesis, AFIT/GAP/ENP/09-M08, Department of Engineering Physics, Air Force Institute of Technology (AU), Wright-Patterson AFB OH, September 1981 (ADA1103970).

Miller, D. M., Schmidt, K. M., Mahan, S. A., McGeehin, J. P., Owen, L. A., Barron, J. A., Lehmkhul, F. and Lohrer, R., 2009: Holocene landscape response to seasonality of storms in the Mojave Desert. *Quaternary International*, Vol. 215, pp 45-61.

Nickling, W. G., 1994: Aeolian sediment transport and deposition. *Sediment Transport and Depositional Processes*, Blackwell Scientific Publications, pp 293-350.

Petty, G., 2004: *A First Course in Atmospheric Radiation*, Sundog Publishing.

Rodgers, S.J., 1968: Evaluation of the dust cloud generated by helicopter rotor blade downwash. United States Army Aviation Materiel Labratories Technical Report 67-81.

Shao, Y., 2004: Simplification of a dust emission scheme and comparison with data. *Journal of Geophysical Research*, Vol. 109.

Shao, Y., 2000: *Physics and Modeling of Wind Erosion*, Kluwer Academic Publishers.

Saho, Y., Lu, H., 2000: A simple expression for wind erosion threshold friction velocity. *Journal of Geophysical Research*, Vol. 105, No. D17, pp 437-443.

Shao, Y., and Raupach, M. R., 1992: The overshoot and equilibrilation of saltation. *Journal of Geophysical Research*, Vol. 97, No. 20, pp 559-564.

Sweeney, M. R., McDonald, E. V., and Etyemezian, V., 2011: Quantifying dust emissions from desert landforms, eastern Mojave Desert, USA. *Geomorphology*, Vol. 135, pp 21-34.

Tanabe, Y. and Saito, S., 2009: Investigation of the downwash induced by rotary wings in ground effect. *Int'l Journal of Aeronautical and Space Sciences*, Vol. 10, No. 1.

US Department of Agriculture, Natural Resources Conservation Service, cited 2014: National Soil Survey Handbook. [Available online at http://soils.usda.gov/technical/handbook].

US Department of Commerce, National Oceanic and Atmospheric Administration, 2005: Field Meteorological Handbook: Surface Weather Observations and Reports, FCM-H1-2005.

US Department of Transportation, Federal Aviation Administration, 2009: Procedures for the Evaluation and Approval of Facilities for Special Authorization Category I and All Category II and III Operations, Order 8400.13D.

Van de Hulst, H.C., 1981: *Light Scattering by Small Particles*, Dover Publications.

Wachspress, D.A., Whitehouse, G.R., Kellr, J.D., McClure, K., Gilmore, P., and Dorsett, M., 2008: Physics based modeling of helicopter brownout for piloted simulation applications. Interservice/Industry Training, Simulation, and Education Conference (I/ITSEC) 2008, Orlando, FL.

Walker, A. L., Liu, M., Miller, S. D., Richardson, K. A., and Westphal, D. L., 2009: Development of a dust source region database for mesoscale forecasting in southwest Asia. *Journal of Geophysical Research*, Vol. 114.

Wolfe, S. A., and Nickling, W. G., 1993: The protective role of sparse vegetation in wind erosion. *Progress in Physical Geography*, Vol. 17, pp 50-68.

Zender, C. S., Newman, D., and Torres, O., 2003b: Spatial heterogeneity in aeolian erodibility: Uniform, topographic, geomorphic, and hydrologic hypotheses. *Journal of Geophysical Research*, Vol. 108, No. D17.

REPORT DOCUMENTATION PAGE

Form Approved
OMB No. 0704–0188

The public reporting burden for this collection of information is estimated to average 1 hour per response, including the time for reviewing instructions, searching existing data sources, gathering and maintaining the data needed, and completing and reviewing the collection of information. Send comments regarding this burden estimate or any other aspect of this collection of information, including suggestions for reducing this burden to Department of Defense, Washington Headquarters Services, Directorate for Information Operations and Reports (0704–0188), 1215 Jefferson Davis Highway, Suite 1204, Arlington, VA 22202–4302. Respondents should be aware that notwithstanding any other provision of law, no person shall be subject to any penalty for failing to comply with a collection of information if it does not display a currently valid OMB control number. **PLEASE DO NOT RETURN YOUR FORM TO THE ABOVE ADDRESS.**

1. REPORT DATE *(DD–MM–YYYY)*	2. REPORT TYPE	3. DATES COVERED *(From — To)*
27–03–2015	Master's Thesis	May 2013 — Mar 2015

4. TITLE AND SUBTITLE

Investigating the Impacts of Particle Size and Wind Speed on Brownout

5a. CONTRACT NUMBER

5b. GRANT NUMBER

5c. PROGRAM ELEMENT NUMBER

6. AUTHOR(S)

Swanson, Brandy A., Captain, USAF

5d. PROJECT NUMBER

5e. TASK NUMBER

5f. WORK UNIT NUMBER

7. PERFORMING ORGANIZATION NAME(S) AND ADDRESS(ES)

Air Force Institute of Technology
Graduate School of Engineering and Management (AFIT/EN)
2950 Hobson Way
WPAFB OH 45433-7765

8. PERFORMING ORGANIZATION REPORT NUMBER

AFIT-ENP-MS-15-M-097

9. SPONSORING / MONITORING AGENCY NAME(S) AND ADDRESS(ES)

Department of Engineering Physics
2950 Hobson Way
WPAFB OH 45433-7765
DSN 785-3636, COMM 937-255-3636
Email: brandy.swanson@afit.edu

10. SPONSOR/MONITOR'S ACRONYM(S)

AFWA

11. SPONSOR/MONITOR'S REPORT NUMBER(S)

12. DISTRIBUTION / AVAILABILITY STATEMENT

DISTRIBUTION STATEMENT A:
APPROVED FOR PUBLIC RELEASE; DISTRIBUTION UNLIMITED.

13. SUPPLEMENTARY NOTES

This material is declared a work of the U.S. Government and is not subject to copyright protection in the United States.

14. ABSTRACT

The impact of particle size and wind speed on brownout cloud development was investigated among various rotary aircraft using Continuum Dynamics, Inc. (CDI) Brownout Analysis Tool, a high physical fidelity brownout model that is used by both U.S. Army Aviation and NASA for Rotorwash analysis. Simulations were run over 125 different combinations of particle size, wind speed, and aircraft type then output data was post-processed to determine a transmissivity and ultimately a visibility value that could be used in developing a severity metric for the brownout clouds generated. For most aircraft types evaluated, stronger wind speeds and smaller particle diameters resulted in denser clouds. Wind speeds greater than 6 m s $^{-1}$ were required to lift particles greater than 30 μm in diameter in most cases

15. SUBJECT TERMS

Brownout, Particle Size, Wind Speed, Rotary Aircraft

16. SECURITY CLASSIFICATION OF:			17. LIMITATION OF ABSTRACT	18. NUMBER OF PAGES	19a. NAME OF RESPONSIBLE PERSON
a. REPORT	b. ABSTRACT	c. THIS PAGE			Lt Col R. S. Wacker, PhD, AFIT/ENP
U	U	U	UU	60	19b. TELEPHONE NUMBER *(include area code)* (937) 255-3636, x4609; robert.wacker@afit.edu